REFORECASTS OF A 2004 ELEVATED CONVECTION EVENT MISFORECAST BY THE ETA MODEL

Martin A. Baxter
Central Michigan University
Department of Geology and Meteorology
Mt. Pleasant, Michigan

Abstract

During the period 24-25 July 2004, elevated convection produced rain totaling up to 5 inches across east-central Missouri. No rain was forecast by the 12 km Eta model over this area. The presence of two concurrent mesoscale convective systems rendered this event a particularly challenging one for numerical weather prediction. An analysis of the physical differences between the model forecast and the observations is initially presented. Deficiencies in the model initial condition and problems inherent in the parameterization of convection are highlighted.

Over the past 6 years, advances in numerical weather prediction and computing power have enabled the development of more sophisticated numerical weather prediction forecasts. Therefore, numerous locally-run forecasts have been generated in an attempt to determine if the original Eta forecast can be improved upon. First, three forecasts conducted on the same grid as the Eta are analyzed to understand the effects of changing the model core and the convective precipitation scheme. The results do not offer substantial betterment over the 2004 Eta forecast, but some improvement is noted. Next, two runs at the convection-allowing grid spacing of 4 km have been generated, with the microphysics scheme varying. Both runs result in more substantial forecast improvement, although some deficiencies remain. Finally, a run with grid spacing of 2 km has been generated. Results indicate that the more realistic simulation of smaller-scale features does not lead to quantitative precipitation forecasts that are notably better than those from the much less computationally expensive 4 km runs.

Corresponding Author: Martin A. Baxter
Dept. of Geology and Meteorology, Central Michigan University
314 Brooks Hall, Mt. Pleasant, MI 48859
E-mail: baxte1ma@cmich.edu

1. Introduction

Quantitative precipitation forecasts (QPF) during the warm season remain one of the foremost challenges of operational forecast models (Olson et al. 1995; Doswell et al. 1996). It is expected that warm season QPF will improve as a result of explicit representation of convection (Fritsch and Carbone 2004). Throughout the last decade, increases in computing power have facilitated the ability to run numerical weather prediction (NWP) models in real-time at grid spacings sufficient to avoid convective parameterization (CP). The National Oceanic and Atmospheric Administration Hazardous Weather Testbed has implemented and evaluated such NWP since 2004 (Kain et al. 2006; Kain et al. 2008), and the National Centers for Environmental Prediction (NCEP) are currently providing 4 km NWP over the contiguous United States and Alaska. Operational meteorologists will now face new challenges in appropriately interpreting such guidance and incorporating it into the forecast process.

Such models feature grid spacings of less than 5 km and are referred to as "convection-allowing", as convection cannot be resolved until horizontal grid spacing approaches 100 m (Bryan et al. 2003; Petch 2006). Nevertheless, 4 km resolution has been observed to sufficiently reproduce much of the structure and evolution of squall-line convective systems depicted in 1 km simulations (Weisman et al. 1997). One of the primary improvements such forecasts have provided over operational models run at resolutions requiring CP is in the representation of the convective mode (Done et al. 2004; Weisman et al. 2008). Subjective evaluation by forecasters confirms this result (Kain et al. 2006).

Convection-allowing models also improve upon the diurnal cycle of convection and its propagation. Carbone et al. (2002) identified "episodes" of warm-season precipitation, in which a sequence of convective events propagate along a corridor over a period of up to 60 h. These episodes are most frequent in midsummer when weaker dynamical forcing is typically present. Convection is initiated in the late afternoon on the eastern slopes of the Rockies and propagates eastward into the Midwest, where the daily maximum precipitation is observed during the overnight hours. Models requiring use of CP do not accurately represent this diurnal cycle of convection over the central U.S. (Davis et al. 2003), and thus do not capture the warm-season rainfall climatology. Idealized simulations using two different CP schemes demonstrate that errors in the timing and propagation of individual convective events lead to the model's inability to simulate the climatology (Davis et al. 2003). Simulations performed in the same study using a convection-allowing model did not experience these deficiencies. Subsequent work by Liu et al. (2006) and Clark et al. (2007) using real data confirm that convection-allowing models better represent the diurnal cycle of convection, and in particular its propagation.

Much of the convection that is responsible for the nocturnal maximum in precipitation over the central U.S. is probably elevated in nature, as half of the convective storms studied in the International H_2O project were found to be elevated (Wilson and Roberts 2006). Elevated convection is typically defined by the lack of air ingested from the near-surface layer (Parker 2008, Glickman 2000). In the case of surface-based convection, the most buoyant parcel may lie above the boundary layer, even if the near-surface parcels contain convective available potential energy (CAPE) (Thompson et al. 2007). The idealized simulations of Parker (2008) confirm that surface parcels containing small amounts of surface-based CAPE will be lifted aloft by the system's cold pool, thus classifying the system as surface-based. Therefore, Corfidi et al. (2008) suggest it is more appropriate to characterize convection along a continuum spanning between purely surface-based and purely elevated forms.

The evolution of the environment in which elevated convection occurs is well known. Building on the work of Colman (1990a; 1990b), and Trier and Parsons (1993), a composite study by Moore et al. (2003) documented the major features and attendant physical processes responsible for 21 central U.S. events of convection that was presumed to be elevated. At the mature stage of the elevated convection, a low-level jet (LLJ) intersects an east-west oriented surface front, acting to transport high θ_e (equivalent potential temperature) air above the cool, stable air north of the boundary. A frontogenetical direct thermal circulation exists aloft at the terminus of the low-level jet, where the elevated convection is most intense. This frontogenesis is thought to be enhanced by deformation resulting from the strengthening LLJ (Trier et al. 2006). This deformation and associated frontogenesis will weaken as the LLJ turns anticyclonically and becomes more parallel to the surface front as morning approaches and the convection dissipates (Trier et al. 2006; Tuttle and Davis 2006).

Evidence exists that models with CP have a particularly difficult time forecasting elevated convection. Of 20 mesoscale convective system (MCS) events simulated at 10 km grid spacing by Jankov and Gallus (2004), those events with the lowest equitable threat scores were cases with elevated convection occurring to the north of a stationary or warm front. CP schemes are developed using assumptions that are heavily based on evidence gathered from surface-based convection (Anderson 2002), and thus may perform particularly poorly in an environment

favoring elevated convection. Many initiations of elevated convection are associated with synoptic or mesoscale wind convergence or confluence at midlevels, which typically cannot be observed (Wilson and Roberts 2006). In synthesis, convection-allowing models may allow improved prediction of elevated convection.

The event analyzed in this paper was selected for retrospective analysis and reforecasting due to the poor performance of the operational Eta at short forecast ranges (18 to 36 h). The event is also one that might be considered challenging for NWP, as it features instances of both convection north of a surface boundary and right along a surface boundary in close proximity. In addition, the convection north of the surface front is maximized at 1800 UTC, rather than during the overnight hours, as is typical for the midsummer months in the central U.S. While studies that objectively and subjectively verify the first generation of operational convection-allowing NWP in a climatological sense are valuable to forecasters, detailed studies of individual events are beneficial as well. The goals of this study are:

- to investigate the reasons for the inaccurate QPF of the 12 km Eta model during a 2004 case of convection north of a surface boundary
- to examine if reforecasts done at both 12 km and the convection-allowing grid spacing of 4 km can improve the QPF
- to speculate on the cause of any resulting improvements for this event

Section two is an overview of the data and methods used. Section three presents an investigation of the 2004 Eta forecast in comparison with the observations and Rapid Update Cycle (RUC) model analyses. Section four features reforecasts of the event using 12 km, 4 km, and 2 km grid spacings, and section five discusses the results and concludes the work.

2. Data and Methods

Reforecasts of the event were conducted using Version 3.1 of the Weather Research and Forecasting (WRF) model, developed at the National Center for Atmospheric Research (Skamarock et al. 2008). 36-hour forecasts were initialized at 0000 UTC 24 July 2004 (from here on, dates and times will be noted in the form of DD/HH UTC, e.g., 24/00 UTC). Both dynamical cores, Advanced Research WRF (ARW) and Non-hydrostatic Mesoscale Model (NMM), were employed. The analysis will focus on the latter 24 hours of this period in order to negate the impacts of model spin up of hydrometeors, although convective systems are often reasonably reproduced within 3-5 h of initialization by convection-allowing models (Weisman et al. 2008). The 12 km domain was identical to that used to distribute the Eta/North American Model (NAM), the NCEP #218 grid. This domain and those used for the 4 and 2 km forecasts is shown in Fig. 1. Nesting of the domains was not used in any of the simulations. The grid spacing in the vertical was comprised of 50 levels, with a model top of 100 mb. Initial and lateral boundary conditions (updated every 3 h) came from the operational Eta model (Black 1994), which has a grid spacing of 12 km and 60 vertical layers to 25 mb. All simulations employed parameterization schemes that are used within the operational Eta/NAM

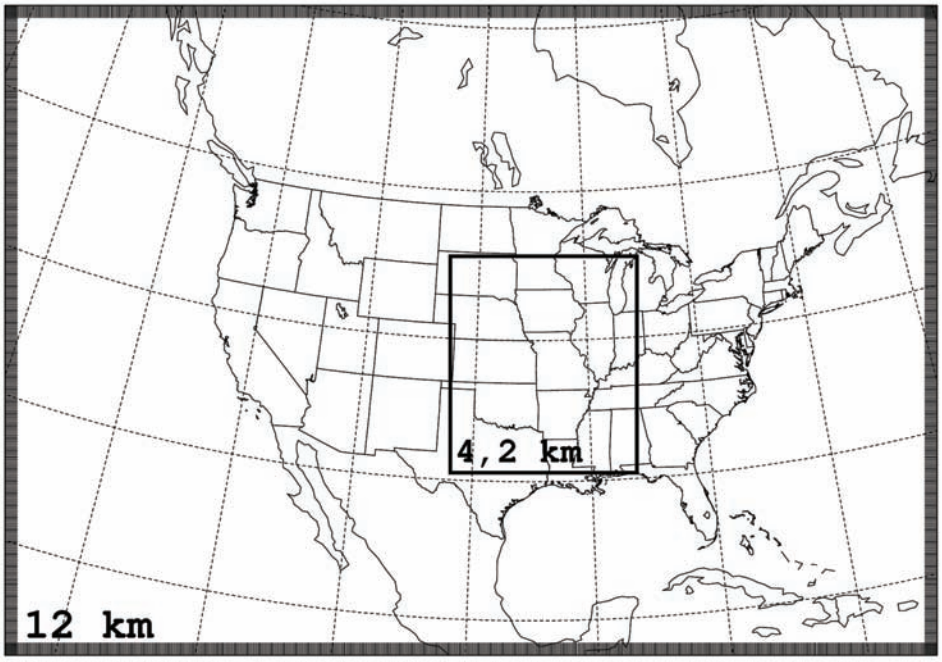

Fig. 1. WRF model domain locations with grid spacing indicated in lower left.

forecasts including the Mellor-Yamada-Janjic planetary boundary layer scheme (Mellor and Yamada 1982), the Geophysical Fluid Dynamics Laboratory longwave and shortwave radiation schemes (Lacis and Hansen 1974), and the NOAH land surface (Ek et al. 2003). A total of six simulations were generated, as follows. Simulation one was configured as a control simulation to mimic the operational Eta model using the WRF-ARW, with Ferrier microphysics (Ferrier et al. 2002) and Betts-Miller-Janic (BMJ) CP (Janjic 1994). Simulation one will be referred to as ARW-BMJ. Simulation two (referred to as NMM-BMJ) switches the model core from ARW to NMM (which is used operationally at NCEP). Simulation three switches the CP scheme to the Kain-Fritsch (KF; Kain 2004), and will be referred to as ARW-KF. Simulation four (referred to as ARW-4-F, where "F" indicates Ferrier microphysics) is identical to simulation one, but was run at 4 km for the domain shown in Fig. 1[1]. Simulation five is identical to simulation four, but switches the microphysics parameterization to the more sophisticated WRF single-moment 6-class microphysics (WSM6) scheme (Hong et al. 2004), and is referred to as ARW-4-WSM. Finally, simulation six (referred to as ARW-2-WSM) is identical to simulation five, but was run at 2 km for the domain shown in Fig. 1. The control ARW-BMJ simulation will not simply reproduce the Eta simulation from 2004, as the model core, numerics, and physics used have been in continuous development over the last 6 years. Despite the fact that the grid spacing used in both the 2004 Eta and the control simulation is equal to 12 km, the models will not be able to resolve the same wavelengths due to the differences previously mentioned. Thus, the effective resolution of the models is fundamentally different, with the WRF-ARW resolving features no smaller than $7\Delta x$, where Δx represents the distance between model grid points, (Skamarock 2004) and the Eta resolving features no smaller than $11\Delta x$ (Vasic et al. 2007). Nonetheless, it is enlightening to examine what effect these changes have on the forecast of the event.

Output from the 20 km RUC (Benjamin et al. 2004) analyses was used as a high resolution, high frequency, dynamically-consistent proxy for the observations, as upper-air observations lack the spatial and temporal resolution necessary for this investigation. The RUC data were carefully compared with upper-air data for the event, and no large-scale errors were observed. Observed precipitation was acquired from the hourly 4 km stage IV precipitation dataset produced by NCEP, which contains some manual quality control from National Weather Service (NWS) River Forecast Centers (Lin and Mitchell 2005). This precipitation was found to be comparable with data from the NWS Cooperative Network. Composite reflectivities from Level III post-processed NWS radar data encompassing 16 elevation scans and interpolated to a 1 km grid were compiled. These observed reflectivities were compared with model-derived instantaneous composite reflectivity (hereafter referred to as simulated reflectivity) calculated using the WRF Post Processor, as discussed in Koch et al. (2005). Since the 2004 Eta did not include a simulated reflectivity product, 3 hourly precipitation must be used. Data from the U.S. National Lightning Detection Network (Orville and Huffines 2001) were used to determine if precipitation was associated with convection. Data used for calculations of quantities involving derivatives were interpolated to the 20 km grid used by the RUC (NCEP #252 grid) to better facilitate comparisons for all forecasts. Despite this interpolation, derived quantities from the reforecasts created with the WRF retain higher magnitude values, likely due to the fundamental differences between the WRF and Eta previously discussed. Therefore, when comparisons are made, the focus will be on the location of the maximized values, rather than their relative magnitudes.

The analysis performed makes use of a calculation of CAPE. As previously discussed, the level chosen for the calculation of CAPE has particular relevance in determining the extent to which the convection is elevated, as discussed further by Rochette et al. (1999). As the parcel levels used for the calculation of CAPE grids contained within the Eta, RUC, and WRF model data differed, recalculation of CAPE was performed using a consistent method for each model. CAPE was calculated using the GEneral Meteorological PAcKage (GEMPAK), with surface-based CAPE calculated using the 2 m temperature and dewpoint. To calculate elevated CAPE, an average CAPE was computed using CAPE values from parcels lifted every 25 mb from 925 to 700 mb. The goal of this calculation was to create a plan view of CAPE in the layer above the surface. CAPE values at the low end of the spectrum will be scrutinized, as Parker (2008) emphasizes the important distinction between parcels with zero CAPE and those with some small amount. The presence of CAPE, coupled with sufficient rising of air to the level of free convection (LFC), indicates that air is rising buoyantly between the LFC and the equilibrium level (EL), regardless of the magnitude of CAPE.

Another variable used in the analysis is potential vorticity (PV). The use of potential vorticity as a framework for atmospheric analysis was presented by Kleinschmidt (1957), and revived by Hoskins et al. (1985). It is possible to recover the balanced wind field throughout the atmosphere when PV is specified over the entire domain. This wind field is said to be "induced" by the PV field. PV over the domain can

[1] An additional 4 km simulation was run using the output from the 12 km ARW-BMJ control simulation as lateral boundary conditions rather than the 2004 Eta. The resulting precipitation fields were similar and thus this simulation will not be presented here.

also be decomposed into individual "pieces" or "anomalies", and the winds induced by each anomaly can be recovered. For instance, a cyclonic (positive) PV anomaly will induce a cyclonic circulation that will be maximized near the level where the PV anomaly is strongest and diminish in strength with increasing distance in both the horizontal and vertical. The distance over which the PV anomalies have influence on the flow increases as the PV anomaly increases in size and as the static stability decreases. Cyclonic PV anomalies develop below the level of maximum latent heating (Raymond and Jiang 1990). A layer average PV was calculated using data every 50 mb from 900 to 700 mb, approximating the layer below the typical location of maximum latent heating occurring during synoptic-scale moist adiabatic ascent (Carlson 1991). The flow induced by the diabatically generated PV has been shown to influence moisture transport (Lackmann 2002; Brennan and Lackmann 2005), and Petterssen frontogenesis (via deformation; Morgan 1999; Korner and Martin 2000; Novak et al. 2009; Baxter et al. 2011). The magnitude of the induced flow can be quantified via a technique known as piecewise PV inversion (Davis and Emanuel 1991). The use of this technique is beyond the scope of this paper; as such information is not available in the operational environment. Instead, the simulated winds, deformation, and Petterssen frontogenesis at 850 mb will be qualitatively compared with the location and magnitude of the 900 to 700 mb average PV. As no tropopause undulation (which represents a positive PV anomaly) is present in this event, it can be surmised that the PV in the 900 to 700 mb layer exerts considerable influence on the 850 mb flow.

3. 2004 Eta Forecast

In comparing the 36 h forecast precipitation accumulated over 24 h (24/12 UTC through 25/12 UTC) by the Eta (Fig. 2a) with the observed precipitation (Fig. 2b); the maxima along the Kansas/Missouri border are in relative agreement. Farther east in the area circled, the Eta predicts no precipitation where 2 to 3 inches fell, and a single NWS Cooperative Observer station reported 5.1 inches. The axis of maximum precipitation is also improperly oriented by the Eta. These represent notable forecast errors, and the fact that the Eta does predict one area of the precipitation well could provide false confidence in other aspects of its forecast.

At the beginning of the 24 h period, 24/12 UTC, a large area of precipitation exists along an inverted trough well north of a surface stationary front (Fig. 3a). The magenta cross in Fig. 3a indicates the coldest infrared cloud tops on Geostationary Operational Environmental Satellite (GOES) imagery (or location of the MCS centroid) at 24/12 UTC, with the extending line indicating the movement of these cloud tops over the next 3 hours (h). Eight lightning flashes are recorded in Kansas and Missouri over the 24/12 UTC through 24/18 UTC period, indicating that this area of precipitation is associated with convection (not shown). A secondary area of precipitation lies right along the front in northeastern Oklahoma. The Eta's 3 h precipitation ending at 24/12 UTC (Fig. 3b) indicates a single maximum south of the main precipitation shield, although the location of the surface front is predicted well as implied by the temperature gradient and wind shift. 6 h later (Fig. 3c), the precipitation that was along the surface front has diminished, while the primary area of convection has propagated to the southeast, with a new MCS (mesoscale convective system) centroid generated on its western flank. The surface front has moved little, though the temperatures south of the front have increased by nearly 20°F. The Eta (Fig. 3d) captures neither the movement of the MCS centroid to the northeast nor the propagation of the convection to the southeast. By 25/00 UTC (Fig. 4a), convection initiates farther south in Oklahoma and Arkansas, resulting in a redefinition of

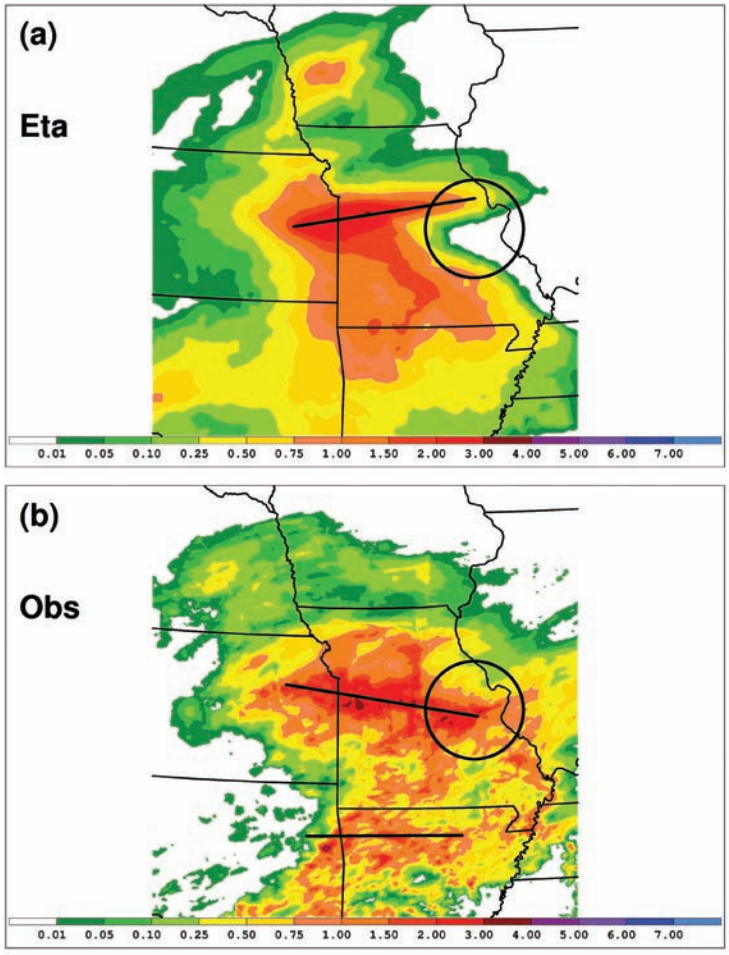

Fig. 2. 24 h accumulated precipitation (shaded; in) for the period 1200 UTC 24 July – 1200 UTC 25 July from the (a) Eta and (b) NCEP Stage IV observations. Black lines indicate axes of maximum precipitation; circles highlight area of primary difference.

the surface boundary farther south. Though the Eta does capture the redefinition of the frontal boundary at 25/00 UTC (Fig. 4b), the precipitation forecast is further degraded, with an incorrect northwest/southeast oriented axis. The northern extent of this convection moves northeast over the next 6 h through 25/06 UTC (Fig. 4c). Through 25/12 UTC, precipitation diminishes across Missouri in both reality and the Eta.

As notable differences exist between the Eta QPF and the evolution of the event on radar, the dynamics and thermodynamics must also be different. Comparison between the Eta analysis at 24/00 UTC (the model initialization time) and the RUC analysis reveals that the Eta suffers from a poor initial condition. While the 250 mb flow pattern and upstream placement of the 500 mb trough are similar (Fig. 5a-b), the 5880 m contour (highlighted) is too far north in the Eta in Missouri and Kansas. The Eta features a stronger vorticity maximum in northern Kansas that is too far to the northwest. This circulation is associated with a mesoscale convective vortex (MCV) related to convection observed in southwestern Kansas 12 h prior. At 850 mb (Fig. 5c- d), the

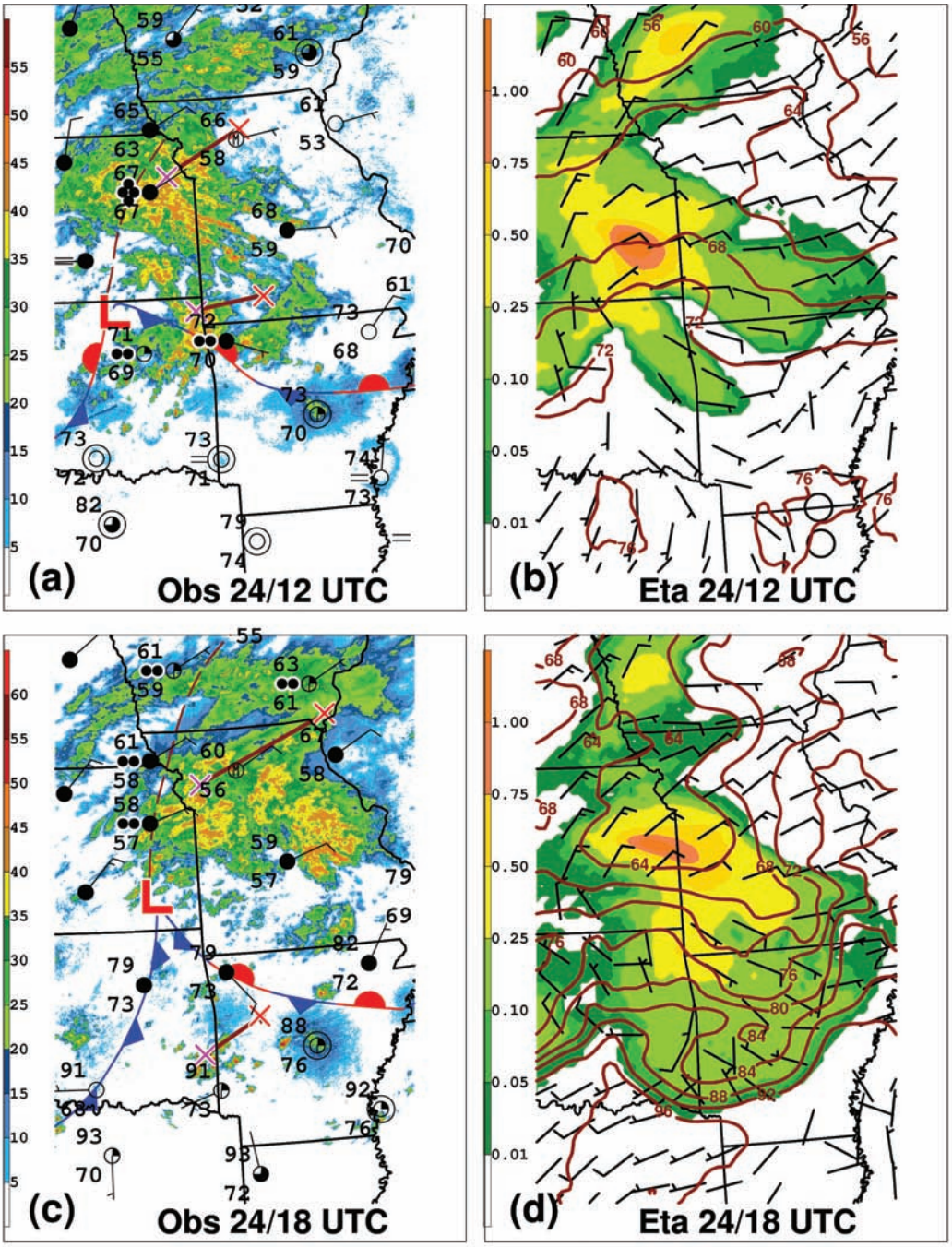

Fig. 3 (a) Level III composite radar reflectivity (shaded; dBZ), surface observations, and surface analysis and (b) Eta 10 m winds (barbs; kts), 2 m temperature (contours; 4°F interval), and 3 h accumulated precipitation (shaded; in) for 1200 UTC 24 July. (c) Same as in (a), and (d) same as in (b), except for 1800 UTC 24 July.

flow pattern is similar, but the θ_e gradient (approximated by the orange line in Fig. 5) is too far north and improperly oriented in the Eta. This is largely due to the Eta's lack of lower θ_e air in central Missouri, which is seen in the RUC. These differences all lead to the reduced likelihood of an accurate forecast over the latter 24 h of the 36 h forecast period.

At 24/18 UTC, convection is occurring north of the surface boundary in both the Eta and reality (Fig. 3c-d), but is found much farther east in reality. As notable differences between the Eta and reality begin to take shape near this time, 24/18 UTC will be a focal point for analysis from this point forward. At this time, the precipitation is in an area of divergence at 250 mb (not shown), and is downstream from a broad trough at 500 mb (Fig. 5e-f). The vorticity maximum in the Eta is in the same location as the 3 h precipitation maximum, while the vorticity maximum in the RUC is associated with the MCS centroid seen on satellite imagery. Further examination indicates that these vorticity maxima are distinct from those seen at 24/00 UTC, as they are associated with the development of a new convective event during the overnight hours.

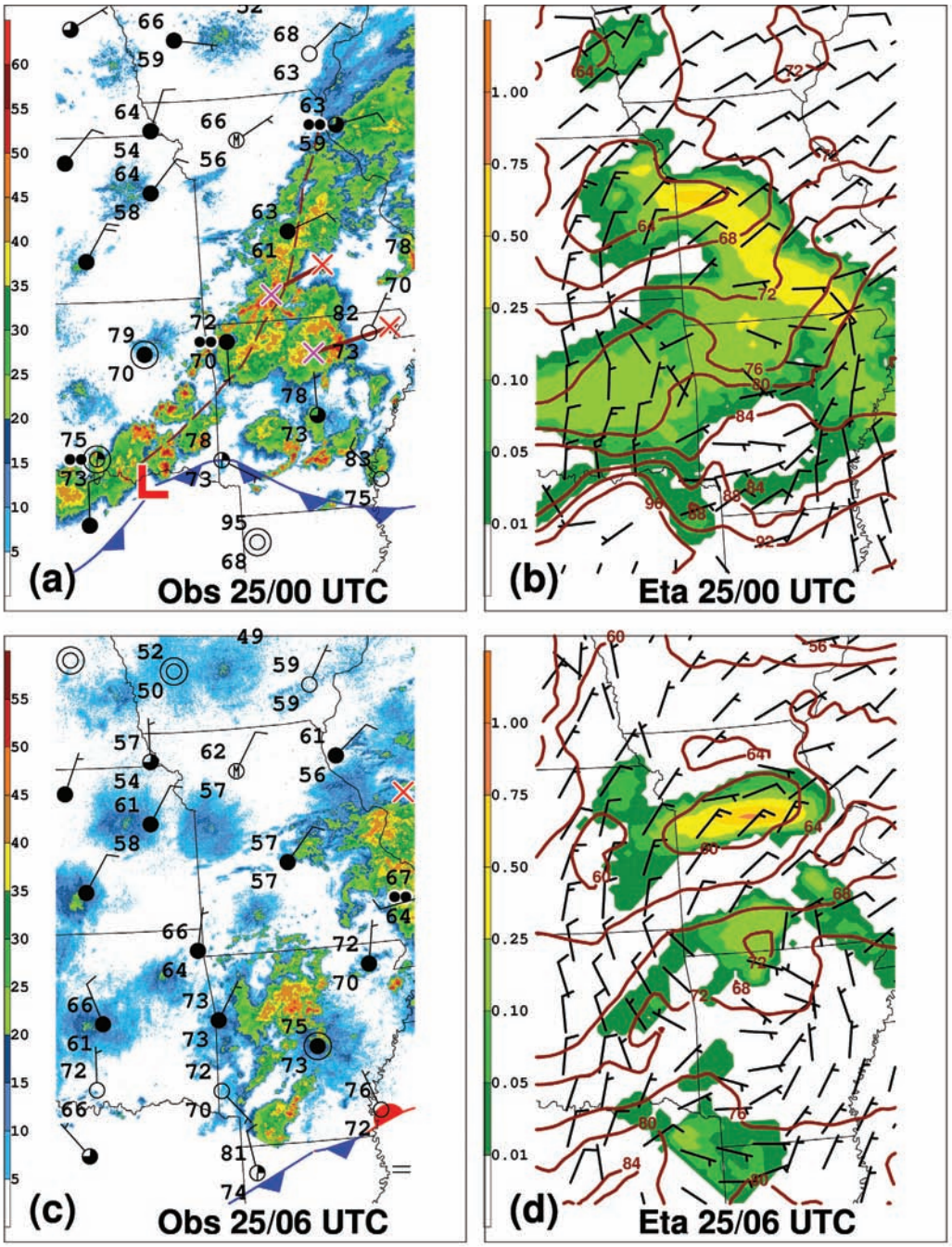

Fig. 4. As in Fig. 3, but for (a) and (b) at 0000 UTC 25 July and (c) and (d) at 0600 UTC 25 July.

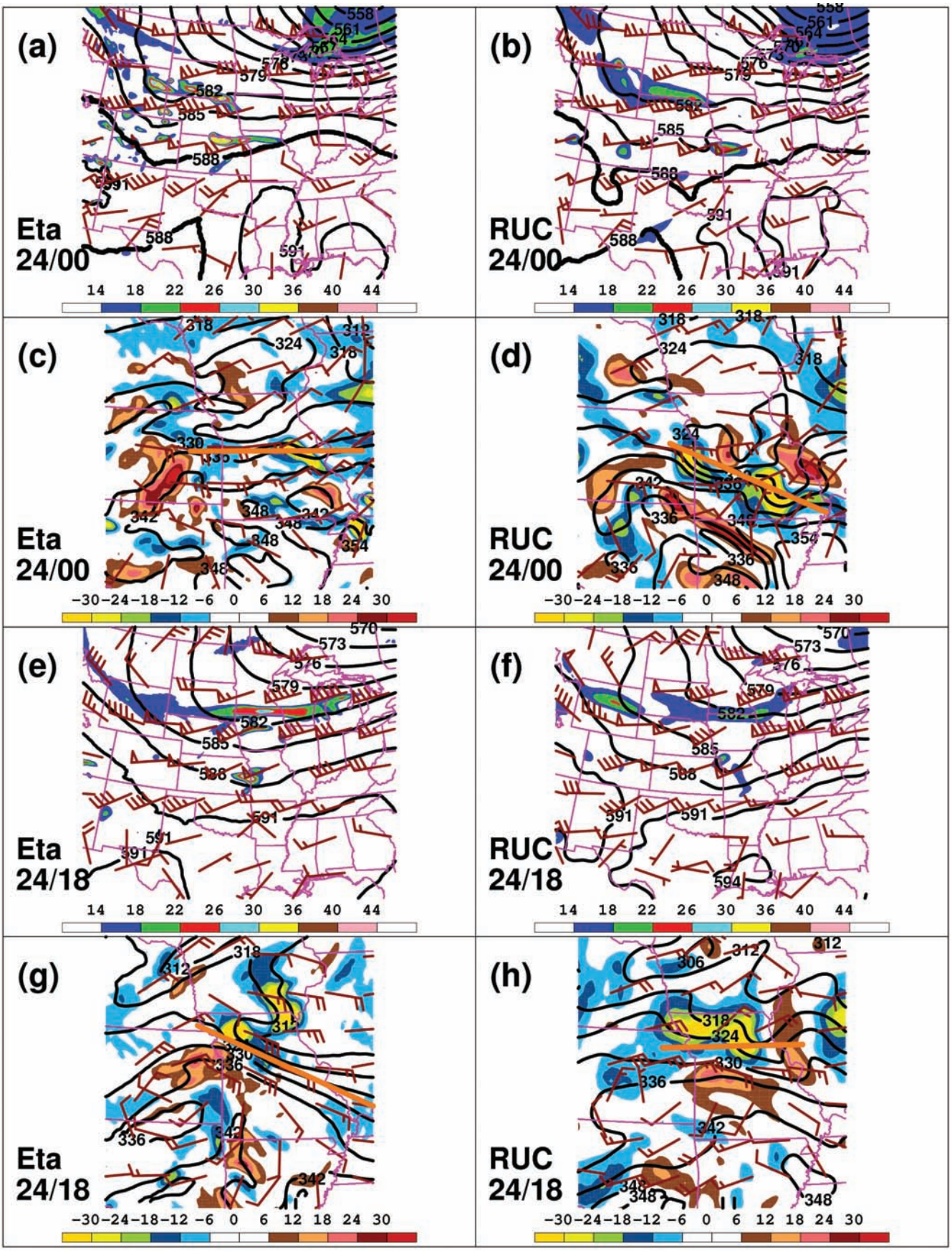

Fig. 5. 500 mb heights (contours; 30 dm) and absolute vorticity (shaded; x 10^{-5} s^{-1}); 250 mb winds (barbs; kts) at 0000 UTC 24 July for (a) Eta and (b) RUC. 850 mb θ_e (contours; 6 K); θ_e advection (x 10^{-1} K h^{-1}); and winds (kts) at 0000 UTC 24 July for (c) Eta and (d) RUC. Lower panels (e-h) identical to that above, only at 1800 UTC 24 July. Orange lines indicate approximate axes of θ_e gradient.

Perhaps the most important differences are seen at 850 mb (Fig. 5g-h). Radar data indicate that convection is occurring along and north of the east-west oriented θ_e gradient in the RUC, while the Eta's precipitation is south of a northwest/southeast oriented θ_e gradient. While both simulate a rather weak 15 to 20 kt low-level jet to the south of this boundary, the orientation of flow with respect to the boundary differs. The flow in the RUC is more perpendicular to the boundary, and is associated with positive θ_e advection extending farther east into central Missouri, while the flow in the Eta is asymptotic to the boundary, with positive θ_e advection present only in western Kansas. In contrast with 18 h prior, it is now the Eta that features lower θ_e air farther south (in northeastern Missouri), causing the boundary to be improperly oriented.

To further explain the differences between the Eta and RUC, moisture and instability are analyzed. At 24/18 UTC in the Eta, the eastern half of the maximum precipitation along the Kansas/Missouri border (Fig. 3d) is in an area of zero surface-based CAPE (Fig. 6a), but positive elevated CAPE (Fig. 6c). The western half of this area of precipitation is in an area with 1 to 25 J kg $^{-1}$ of surface-based CAPE and positive elevated CAPE. In east-central Missouri, surface-based CAPE is present, but no elevated CAPE exists. The air at the surface (Fig. 6a) and the low-levels (Fig. 6b) is not saturated in east-central Missouri, and no precipitation is forecast here (Fig. 6e). The RUC depicts near surface air parcels in central Missouri with 1 to 25 J kg^{-1} of CAPE (Fig. 6b), indicating that convection observed in this area (Fig. 3c) is actually surface-based. In eastern Missouri, where reflectivities are slightly higher in magnitude (Fig. 3c), surface-based CAPE is essentially zero. Positive values of low-level average (925 to 700 mb) CAPE (Fig. 6d) extend over this area, suggesting that this convection is elevated in nature. The gradient in saturation in the RUC is in eastern Missouri, both at the surface (Fig. 6b) and the low-levels (Fig. 6d). In both datasets, the 6 h precipitation ending at 24/18 UTC ends along the gradient in saturation, which correlates well with the elevated CAPE (Fig. 6e-f). Although this analysis does confirm that a large portion of the convection in the model was indeed elevated, this comparison illustrates the complexities involved in categorizing convection as "elevated" or "surface-based".

The pattern of elevated CAPE is particularly closely aligned with the area of maximum 3 h precipitation in the Eta (Fig. 6e). In this area, 50 to 70% of the total precipitation is due to the CP scheme, a local minimum. The balance between stratiform and convective precipitation will vary with resolution, parameterization schemes used, and degree of convective organization (Belair and Mailhot 2001). It is unknown what the appropriate value should be in an environment where convection is embedded within grid-scale, stratiform precipitation, as the presence of both indicates that the CP and microphysics scheme should be producing precipitation in the same location. Therefore, it is possible that the BMJ scheme is not properly representing the effects of the convection on the resolved scales, which can influence the propagation of the convection.

As discussed in section two, latent heating associated with the convection results in low-level PV production. At 24/18 UTC, both the Eta and RUC produce PV anomalies (Fig. 7a-b) maximized in the vicinity of precipitation in eastern Kansas (Fig. 3c-d). The Eta does not contain the PV seen in the RUC, which extends along the axis of observed precipitation in central Missouri. In both datasets, the observed cyclonic circulation at 850 mb is well correlated with the layer-averaged PV anomalies, lending credence to the likelihood that this flow was induced by these particular PV anomalies. Petterssen frontogenesis is maximized along the northern edge of each anomaly (Fig. 7a-b). A positive contribution to frontogenesis results when the long axis of deformation is collocated with the thermal gradient. The flow surrounding the PV anomaly is associated with the axes of deformation (Fig. 7c-d), as marked by the orange lines. The relationship between the PV anomalies and the thermal gradients (Fig. 7c-d) is more tenuous, as the thermal gradient is strongest north of the PV anomaly in the Eta and right along the PV anomaly in the RUC. The long axis of deformation is collocated with the thermal gradient in the RUC through central Missouri, while little collocation of the two takes place in the Eta.

In the Eta, potential problems with the parameterization of convection itself, and insufficient downstream instability and moisture are associated with the lack of propagation of the convection. The deformation associated with the diabatically-generated PV remains close to the area of stationary convection and not collocated with the thermal gradient. In the RUC, as cyclonic flow is collocated with a diabatically generated PV anomaly, it appears that the convection itself may be inducing deformation that *contributes to* (but does not completely explain) the existence of frontogenesis farther east. The fact that no frontogenesis is apparent in central Missouri 6 hours earlier when widespread convection had yet to enter this area lends credence to the idea that as convection propagated to the southeast; it served to alter the mesoscale environment via the generation of frontogenesis. The flow from the south (the LLJ circled in Fig. 7b) is perpendicular to this frontogenesis, thus leading to ascent of high θ_e air to continue fueling the convection.

A cross-section taken on a N-S line through

Continued page 14

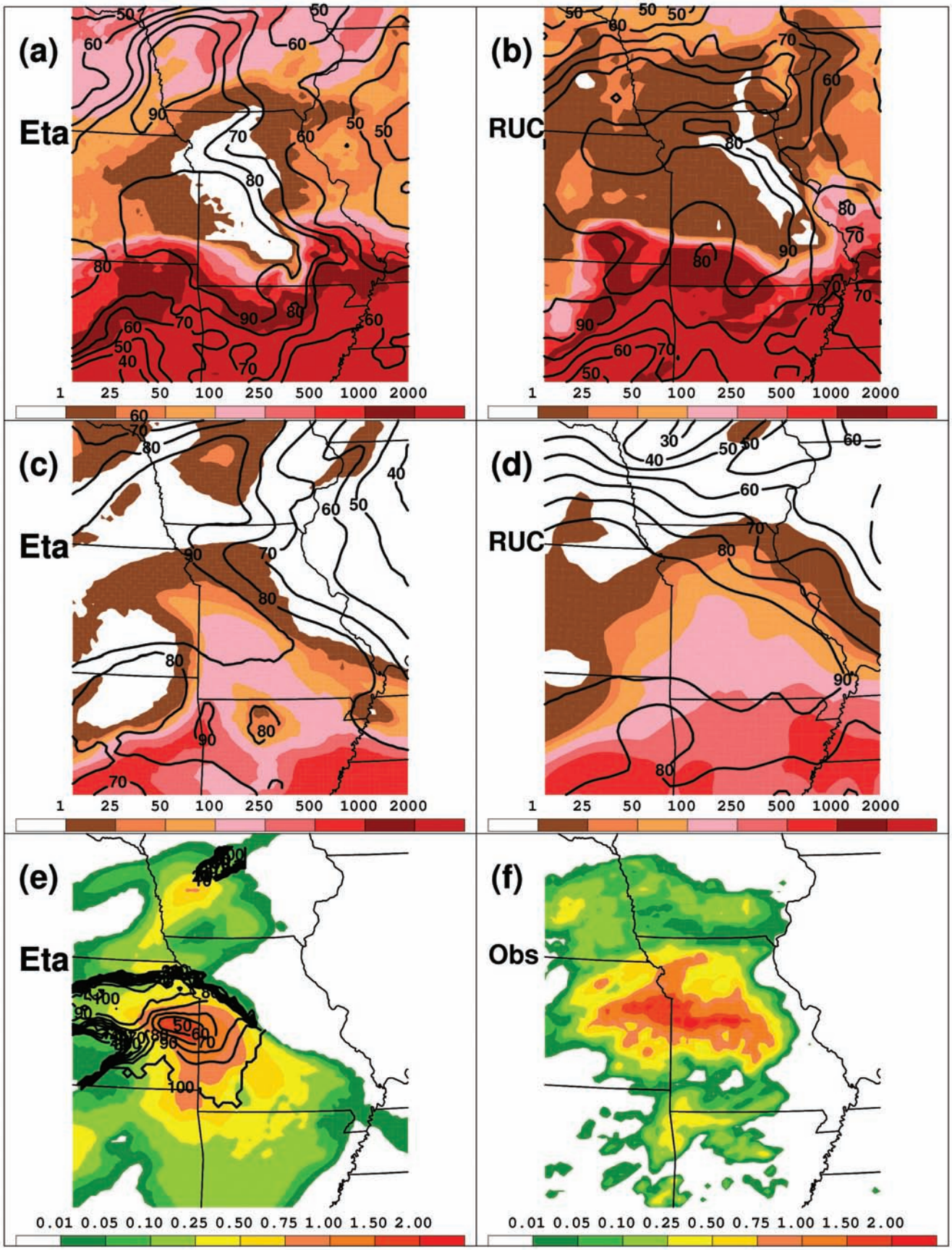

Fig. 6. 2 m relative humidity (contours; 10%), surface CAPE (shaded; J kg^{-1}) at 1800 UTC 24 July for (a) Eta and (b) RUC . (c) and (d) as above, but for 925-700 mb average relative humidity and CAPE. (e) Eta 6 h accumulated precipitation (shaded; in), ending 1800 UTC 24 July and percentage of total which was produced via the convective scheme (contours; 10%). (d) Observed 6 h accumulated precipitation ending 1800 UTC 24 July.

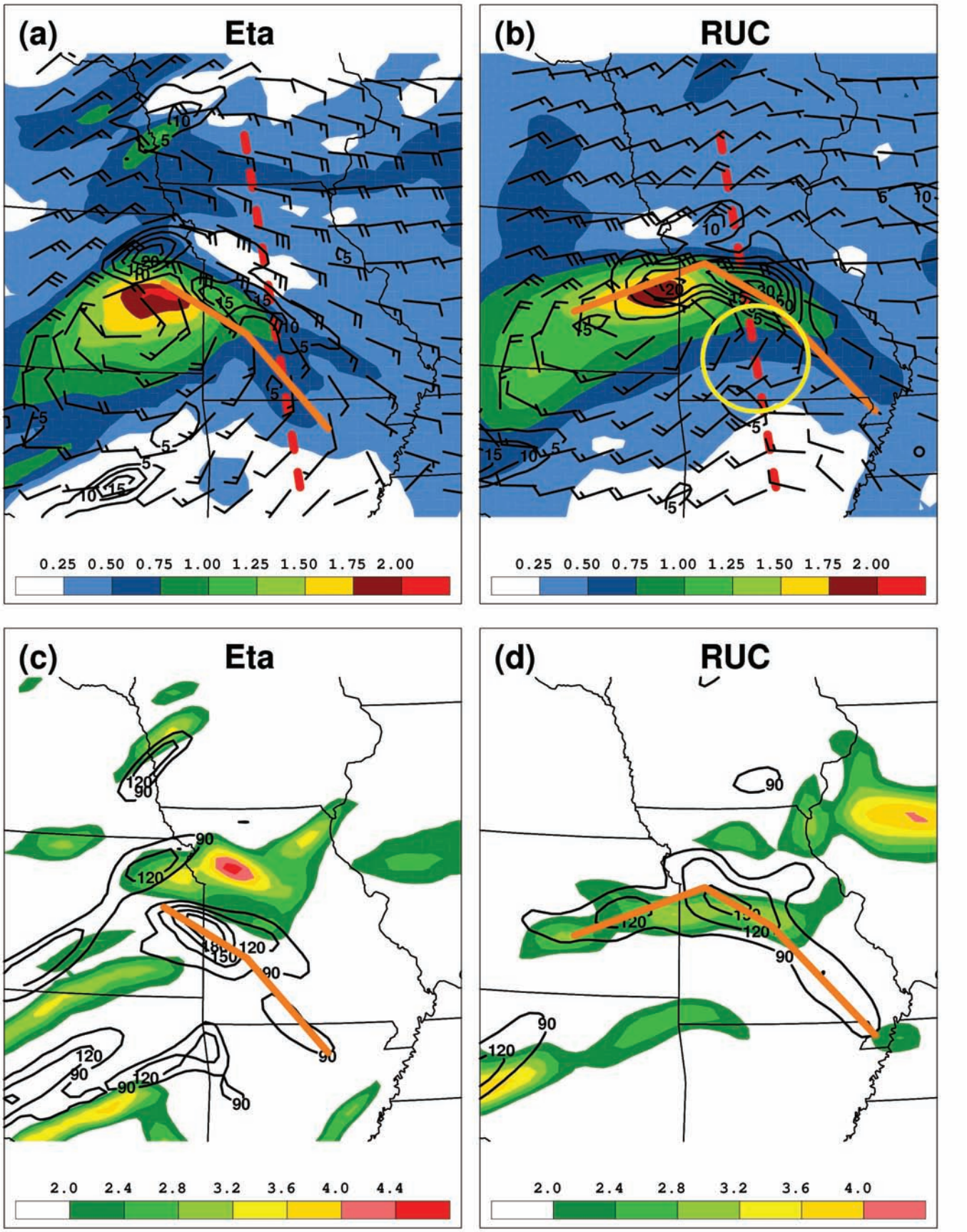

Fig. 7. 900-700 mb average PV (shaded; PVU), 850 mb winds (barbs; kts), and frontogenesis (contours; 5 K 100 km^{-1} 3 h^{-1}) at 1800 UTC 24 July for (a) Eta and (b) RUC. 850 mb temperature gradient (shaded; °C 100 km^{-1}) and deformation (contours; 30x10^{-5} s^{-1}) at 1800 UTC 24 July for (c) Eta and (d) RUC. Red dashed line indicates cross section location in Fig. 8. Orange lines indicate primary axes of deformation. Circle highlights the nose of the LLJ.

central Missouri (indicated by the red line on Fig. 7a-b) depicts the *lack* of a strong, vertically coherent axis of frontogenesis in the Eta at 24/18 UTC (Fig. 8a). These features *are* present within the RUC (Fig. 8b). Positive θ_e advection is also strong and deep along the southern side of the frontogenesis in the RUC. Also of note is the stronger negative θ_e advection that is observed in the RUC along the northern side of the frontogenesis. This is seen in plan view in Fig. 5h, and may relate to the more northerly flow seen in the RUC, as well as the low-level rain cooled air present in this area (Fig. 3c) that is not forecast by the Eta (Fig. 3d). This negative θ_e advection is evidence that the deformation pattern associated with the diabatically-generated PV is not the *only* contributor to frontogenesis in the RUC in central Missouri. The Eta does have lower θ_e values in northern Missouri, but the flow is parallel to the boundary, and thus is less likely to contribute to frontogenesis.

Although the initial condition used for the Eta forecast was poor, and the presence of lower θ_e air in northern and eastern Missouri inhibited the propagation of convection, it does appear that the CP scheme also played a role in the poor forecast. Thus, new simulations using the WRF model were performed to see if further model development, the use of a different model core, and the use of a different CP scheme improved upon the Eta forecast.

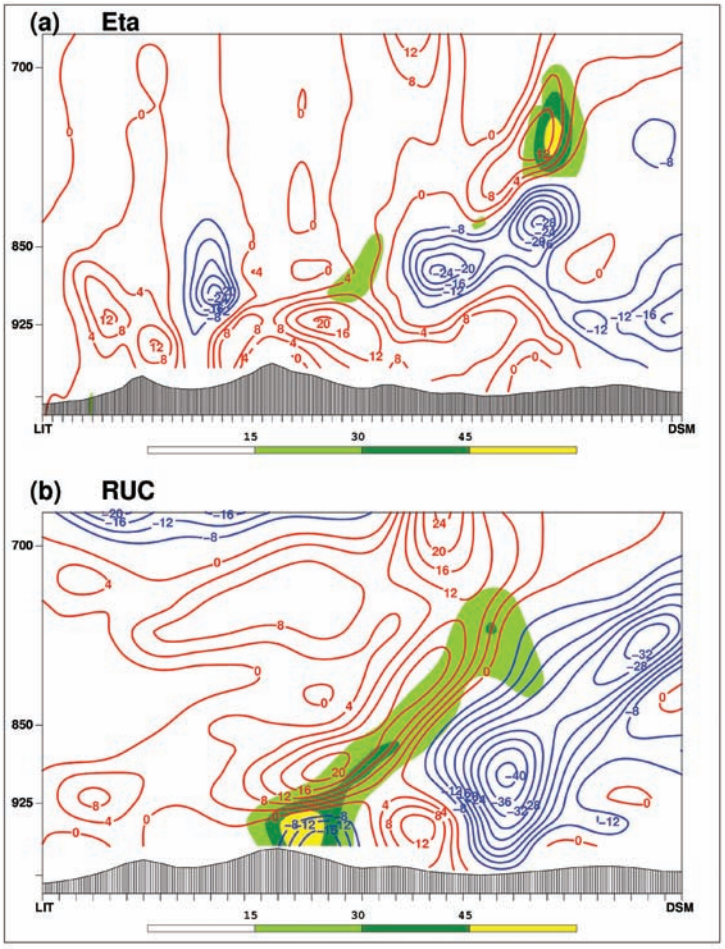

Fig. 8. Cross section at 1800 UTC 24 July from Little Rock, AR to Des Moines, IA as indicated in Fig. 7, with θ_e advection (contours; positive values in red, negative in blue; x 10^{-1} K h^{-1}) and frontogenesis (shaded; K 100 km^{-1} 3 h^{-1}) shown.

4. Reforecasts

a. 12 km runs

As discussed in section two, three reforecasts with 12 km grid spacing were performed. The ARW-BMJ (Fig. 9a) depicts two distinct east-west tracks of precipitation, in northern Missouri and Kansas and southern Missouri and Kansas, as marked. The 2004 Eta does not depict two different tracks (Fig. 2a), as were observed (Fig. 2b). Both the 2004 Eta and the ARW-BMJ fail to predict the observed precipitation in eastern Missouri (Fig. 2b). The NMM-BMJ (Fig. 9b) run does feature two tracks of precipitation, but the southernmost track contains precipitation amounts far in excess of what was observed. The ARW-BMJ also contains higher amounts than observed along the southern track, but not to the extent in magnitude and areal coverage seen in the NMM-BMJ. The NMM-BMJ does feature precipitation in eastern Missouri, but further examination of simulated reflectivities (not shown) reveals that this precipitation is a result of the erroneous precipitation along the southern track. As this precipitation in eastern Missouri resulted from the northern track in reality, the NMM-BMJ will not be investigated further. The ARW-KF (Fig. 9c) looks markedly different than the ARW-BMJ, highlighting the high degree of sensitivity to the choice of CP scheme for this event, as is often observed (e.g. Wang and Seaman 1997). It is difficult to discern the presence of two precipitation tracks, and the precipitation in eastern Missouri is less than that seen in the ARW-BMJ.

Examination of simulated reflectivity provides greater insight into the development of the two tracks of precipitation in the ARW-BMJ. The more intense precipitation in southeastern Kansas (Fig. 10a) corresponds with the precipitation which is observed along the surface front at 24/12 UTC (Fig. 3a). In reality, this precipitation diminished by 24/18 UTC (Fig. 3c), followed by redevelopment of precipitation in northern Arkansas and southern Missouri (Fig. 4a). Two tracks do not appear in the ARW-KF (Fig. 10b, d, f, h), and thus the reforecast more closely resembles that of the 2004 Eta. In the ARW-BMJ, the southern area of precipitation maintains itself through 25/06 UTC (Fig. 10c, e, g). The northern area of precipitation in the model is shifted to the west versus reality at each time shown, and does not reach eastern Missouri. Despite the inaccuracies in precipitation amounts, and the lack of precipitation in eastern Missouri,

the appearance of two tracks of precipitation within the ARW-BMJ indicates a forecast more consistent with what actually occurred in comparison with the 2004 Eta.

At 24/18 UTC, the patterns of surface relative humidity and CAPE are similar for both the ARW-BMJ (Fig. 11a) and ARW-KF (Fig. 11b), which are in turn similar to the 2004 Eta (Fig. 6a). The same generally holds true for elevated CAPE and low-level average relative humidity (Fig. 11 c-d, and Fig. 6c). The ARW-BMJ elevated CAPE is locally diminished in southwest Missouri, in the same location where precipitation is simulated. Less than 20% of the total precipitation results from the BMJ scheme throughout the area of precipitation (Fig. 11e), even in southern Missouri where elevated CAPE remains and a precipitation maximum exists. The fact that less convective precipitation is produced than stratiform precipitation in an area where CAPE exists could indicate that the CP scheme is not removing enough instability. When this occurs, excess instability is removed on the grid scale, leading to excess heating aloft that results in further low-level convergence and more precipitation in-situ (Zhang et al. 1988). This suggests that the model may not be realistically representing the convection, although this area of convection does move within the ARW-BMJ. In the ARW-KF (Fig. 11f), less than 40% of the total precipitation results from the KF scheme in the region of maximum precipitation along the gradient of elevated CAPE, but precipitation to the south of the maximum precipitation is generated predominantly by the KF scheme. Precipitation amounts are not considerably overdone in the ARW-KF, and the precipitation forms and dies in roughly the same location without the existence of two tracks. These differences among the three models (2004 Eta, ARW-BMJ, and ARW-KF), suggest that the manner in which a CP is formulated and how the CP interacts with the other physical parameterizations will have a large impact on the resulting total precipitation and reflectivity fields, as previously discussed in Gallus (1999) and Gallus and Segal (2001).

As expected, the two tracks of precipitation are associated with two individual PV anomalies in the ARW-BMJ (Fig. 12a), and the single track of precipitation is associated with a single PV anomaly in the ARW-KF (Fig. 12b). All the PV anomalies are collocated with either cyclonic circulations or cyclonic wind shifts, which are associated with areas of deformation (Fig. 12c-d). Both reforecasts have a strong thermal gradient in northern Kansas and Missouri (Fig. 12c-d), but only the ARW-BMJ contains strong deformation here, resulting in stronger frontogenesis (Fig. 12a-b). These fields in the ARW-KF are quite similar to those seen in the 2004 Eta (Fig. 7a-c), except that the deformation in southern Kansas and Missouri is now collocated with the thermal gradient, producing frontogenesis farther south in the ARW-KF. The most striking difference between the ARW-BMJ and the 2004 Eta is the strong deformation collocated with the thermal gradient in southern Missouri seen in the ARW-BMJ, in the area of heaviest precipitation. Strong frontogenesis is produced here, with a 15 to 30 kt LLJ flowing perpendicular to the frontogenesis from the south.

Continued page 18

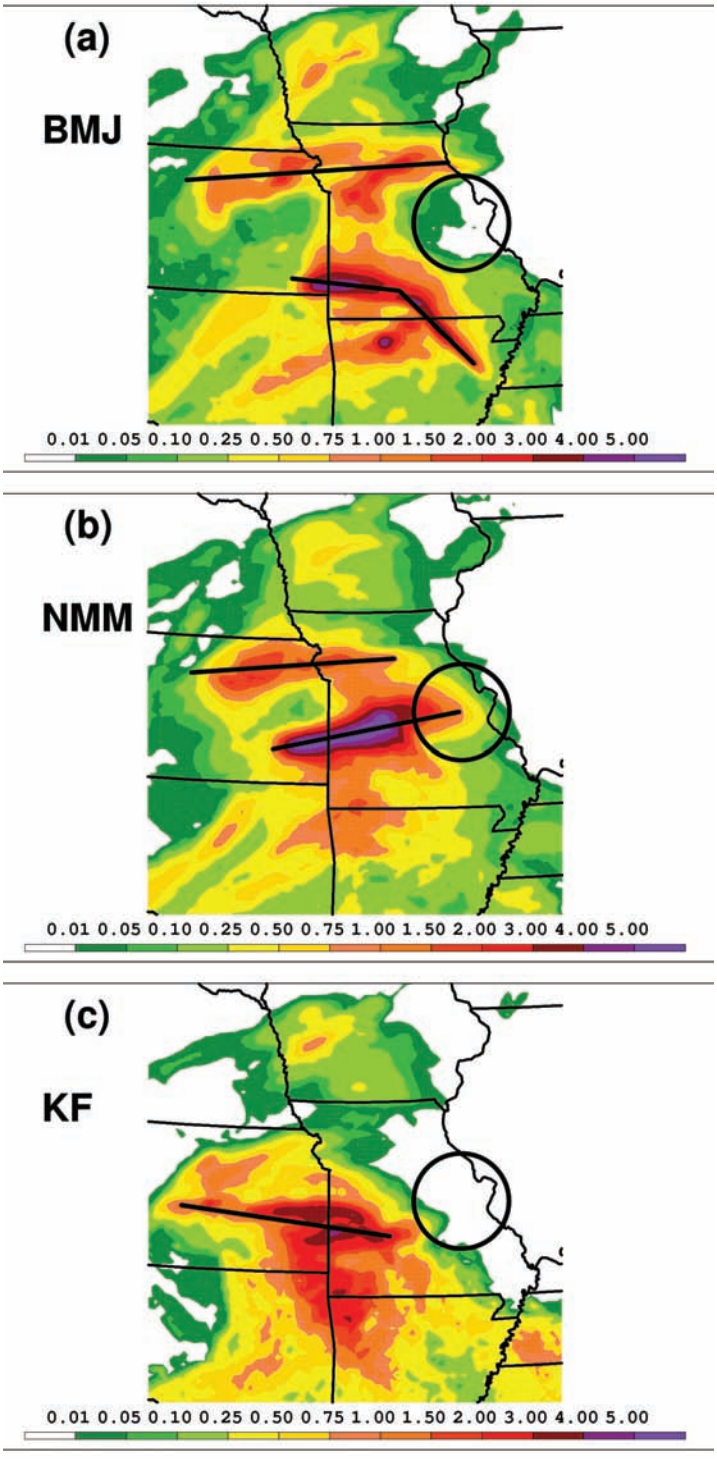

Fig. 9. As in Fig. 2, but for (a) ARW-BMJ, (b) NMM-BMJ, (c) ARW-KF.

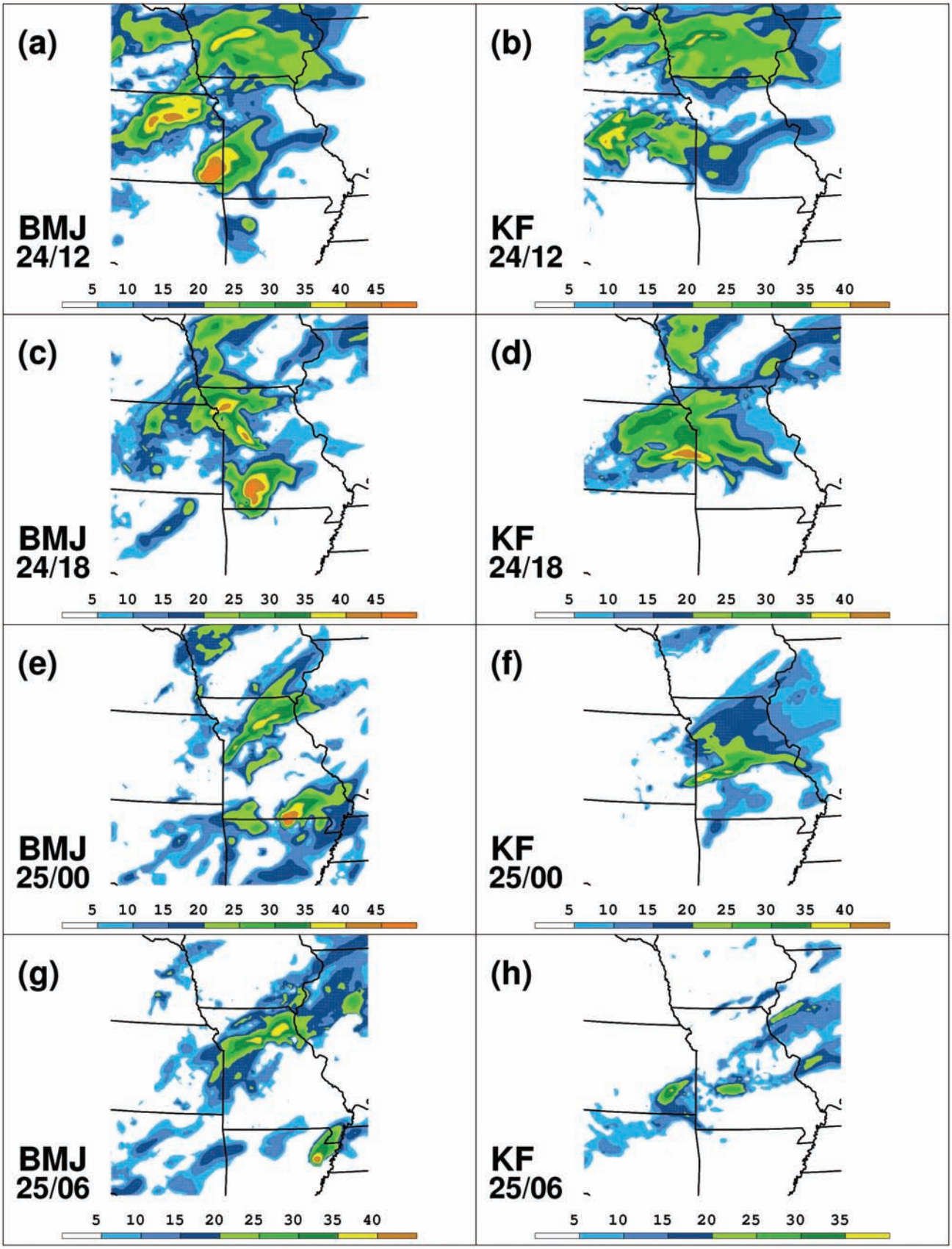

Fig. 10. Model-derived instantaneous composite reflectivity (shaded; dBZ) at 1200 UTC 24 July from ARW-BMJ (a) and from ARW-KF (b). Remaining panels same as in (a-b), except (c-d) at 1800 UTC 24 July, (e-f) at 0000 UTC 25 July, and (g-h) at 0600 UTC 25 July.

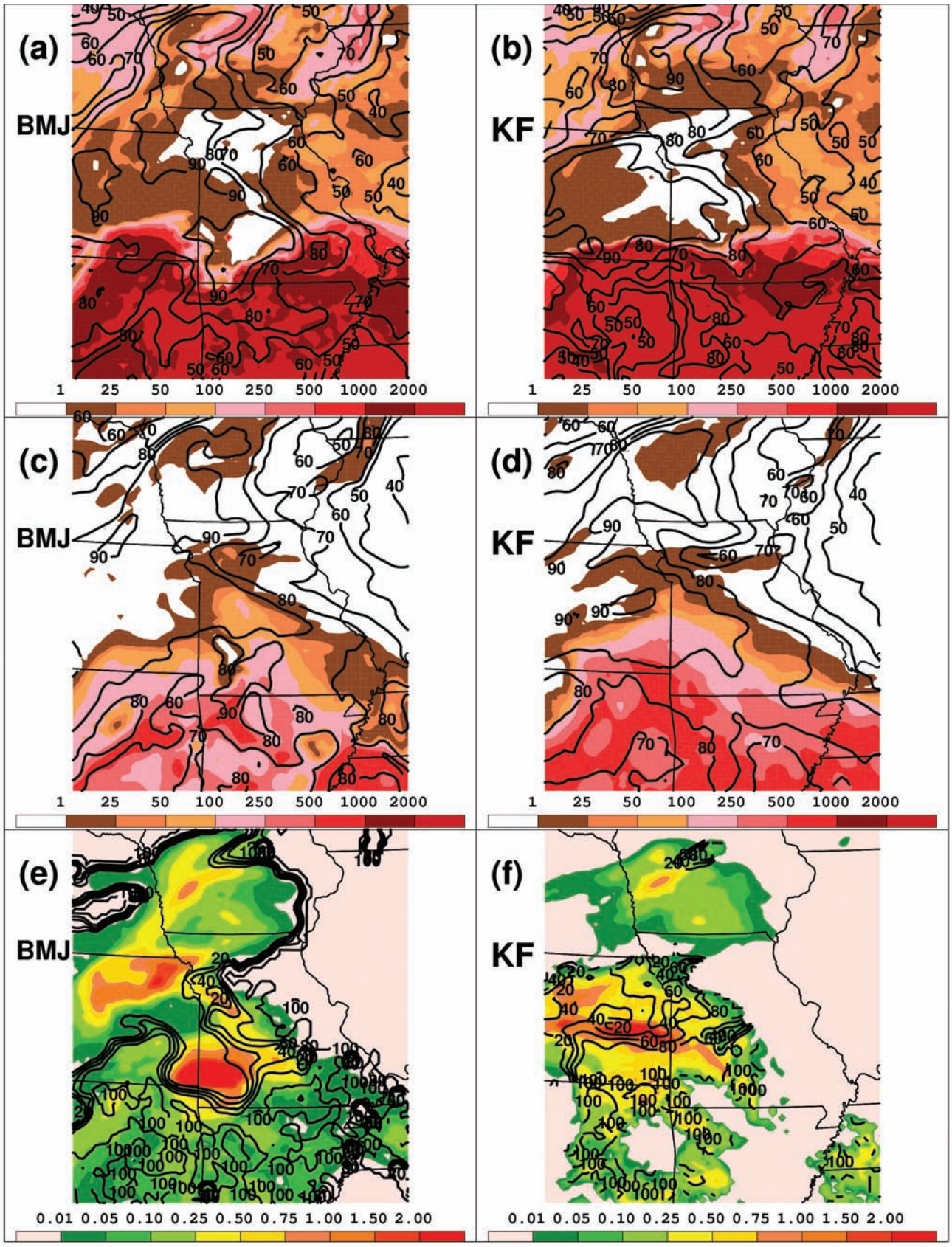

Fig. 11. As in Fig. 6, but using ARW-BMJ (left side) and ARW-KF (right side). Note that Fig. 6f depicts observed precipitation, while (f) shows model simulated precipitation.

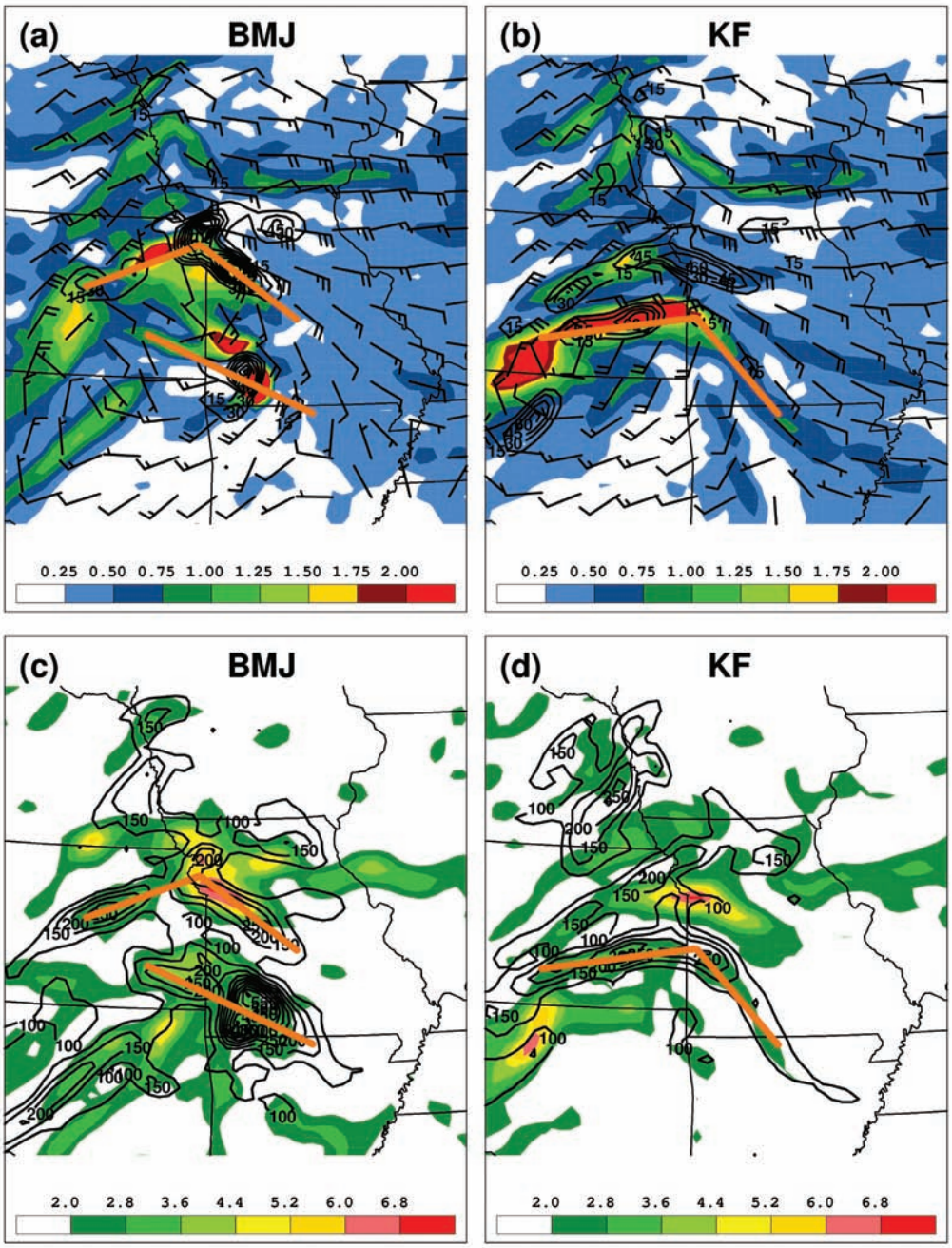

Fig. 12. As in Fig. 7, but using ARW-BMJ (left side) and ARW-KF (right side). Frontogenesis in (a) and (b) is contoured every 15 K 100 km^{-1} 3 h^{-1} and deformation in (c) and (d) is contoured every 50x10^{-5} s^{-1}.

It is clear why heavy precipitation is maintained here in the ARW-BMJ, while it was not observed to continue in reality, as the RUC depicts no frontogenesis here.

Although the ARW-BMJ did forecast two distinct areas of precipitation that were observed in reality and were not forecast well by the 2004 Eta, neither the ARW-BMJ nor the ARW-KF predicted precipitation in eastern Missouri. Though the ARW-BMJ simulation was more realistic, it apparently suffered from an underactive CP scheme and thus resulted in the inappropriate maintenance of the southern track of precipitation. The ARW-BMJ (and the NMM-BMJ) illustrate that while some aspects of a forecast can be correct, others can be in error. Despite the problems related to the CP schemes, the presence of two tracks of precipitation in the ARW-BMJ reforecast provides valuable information to the forecaster which was not seen in the 2004 Eta. The fact that the ARW-KF reforecast was substantially different than the ARW-BMJ indicates that this situation is highly sensitive to the manner in which convection is parameterized. This illustrates that there is a high degree of uncertainty in the forecast of this event, and suggests that elimination of the CP scheme in the simulation could reduce the uncertainty.

b. 4 km runs

In light of the myriad of potential benefits derived from generating forecasts using convection-allowing grid spacing, two simulations were run at 4 km with no CP. As described in section two, the microphysics scheme was varied from Ferrier in the ARW-4-F run to WSM6 in the ARW-4-WSM run. The WSM6 scheme maintains ice phase hydrometeors as separate quantities. This more sophisticated treatment may provide benefit in higher resolution simulations (Hong et al. 2004). In this case, the QPF was generally similar for both runs (Fig. 13a-b). The use of WSM6 microphysics resulted in precipitation slightly farther east and the reduction of some areas of maximum precipitation, both more realistic outcomes. Thus, it is this reforecast that will be further examined. The axis of forecast precipitation is nearly identical to that of the observed precipitation (Fig. 2b). Though the precipitation does not reach the Missouri/Illinois border, it is much closer to this area than any of the previously discussed forecasts. Comparison of simulated reflectivity (Fig. 14) with observed reflectivity (Fig. 3a-c and Fig. 4a-c) indicates noteworthy improvements as well, particularly at 24/12 UTC and 24/18 UTC. As in the ARW-BMJ reforecast and the observations, two tracks of precipitation are present. Along the southern track, precipitation diminishes in areal coverage between 24/12 UTC and 24/18 UTC, and then reintensifies at 25/00 UTC, as was observed. Along the northern track, reflectivity values greater than 40 dBz in east-central Missouri indicate that there must be sufficient moisture, lift, and instability to maintain precipitation here.

While a portion of Missouri does have essentially zero surface CAPE (Fig. 15a), the coverage of areas with at least some surface CAPE is comparable to that seen in the RUC (Fig. 6b). Elevated CAPE (Fig. 15b), while not as far north in areal coverage as the RUC (Fig. 6d), does extend farther north in east-central Missouri compared to all other forecasts (Fig. 6c, 11c-d). The surface (Fig. 15a) and low-level relative humidity (Fig. 15b) gradients in this reforecast are also farther east, again comparable to those in the RUC (Fig. 6b-d). It is apparent that the enhanced resolution of the model has resulted in major changes to the physical processes responsible for this event. It is not entirely clear how this has occurred, other than to speculate that 18 h into the forecast, the low-level moisture field is better resolved and has evolved in a more realistic way.

Two sets of PV anomalies are present in association with the northern and southern areas of precipitation (Fig. 16a). The PV in central Missouri is collocated with the axis of deformation (Fig. 16b). There exists some overlap between the axis of deformation and the thermal gradient

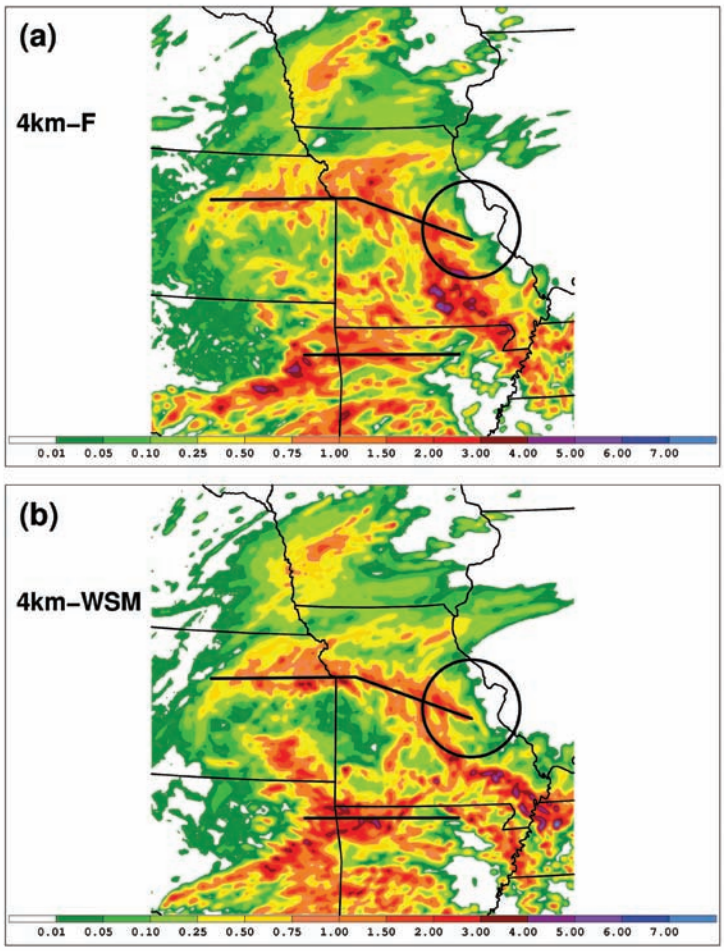

Fig. 13. As in Fig. 2, but using (a) ARW-4-F and (b) ARW-4-WSM.

(Fig. 16b), resulting in the production of frontogenesis (Fig. 16a) along and north of the area of PV. The flow in south-central Missouri representing the LLJ is perpendicular to the axis of frontogenesis in central Missouri (circled in Fig. 16a), as seen in the RUC (circled in Fig. 7b), and is not asymptotic to it, as seen in all other forecasts (Fig. 7a, 12a-b). The PV in the south is only collocated with the axis of deformation in southeastern Kansas. The PV in southern Missouri is in an area where previously persistent heavy precipitation (Fig. 14a) has dissipated over the previous 6 h, leaving a strong PV anomaly. The convection in northwest Arkansas is rapidly propagating, and thus does not generate a strong PV anomaly. The PV anomaly in southern Missouri may be responsible for the deformation visible in northwest Arkansas, as the influence this anomaly has on the flow will be greater in the less stable air south of the surface front.

The fact that the moisture, lift, and instability fields are more comparable to those seen in the RUC indicates that the lack of a CP scheme and the increased resolution have improved the realism and accuracy compared with all other forecasts investigated here. The specific reasons for the improvement brought on by the convection-allowing reforecast (ARW-4-WSM) are not derived in

this study. The convection is observed to propagate downstream more realistically, a property noted by other studies as discussed in section two. As the convection propagates, diabatically generated PV anomalies result that induces deformation along the thermal gradient, promoting frontogenesis. As in the RUC, 6 h prior at 24/12 UTC, frontogenesis in central Missouri is weaker prior to the propagation of convection into the area. At 24/18 UTC, when convection is ongoing in central Missouri, frontogenesis develops coincident to the convection. This frontogenesis serves as a lifting mechanism for the high θ_e air within the LLJ streaming northward from the south, resulting in the maintenance of the convection. In this case, the orientation of the LLJ appears to be influenced by the development of convection and a PV anomaly to the south of the east-west oriented convection in central Missouri. Conceptually, this PV anomaly will induce southerly flow on its eastern flank, consistent with what was observed in the ARW-4-WSM. The ARW-BMJ contains this feature as well, but it is improperly simulated, as discussed. This PV anomaly could be too small in scale to be resolved by the RUC, though its upscale influence may remain visible.

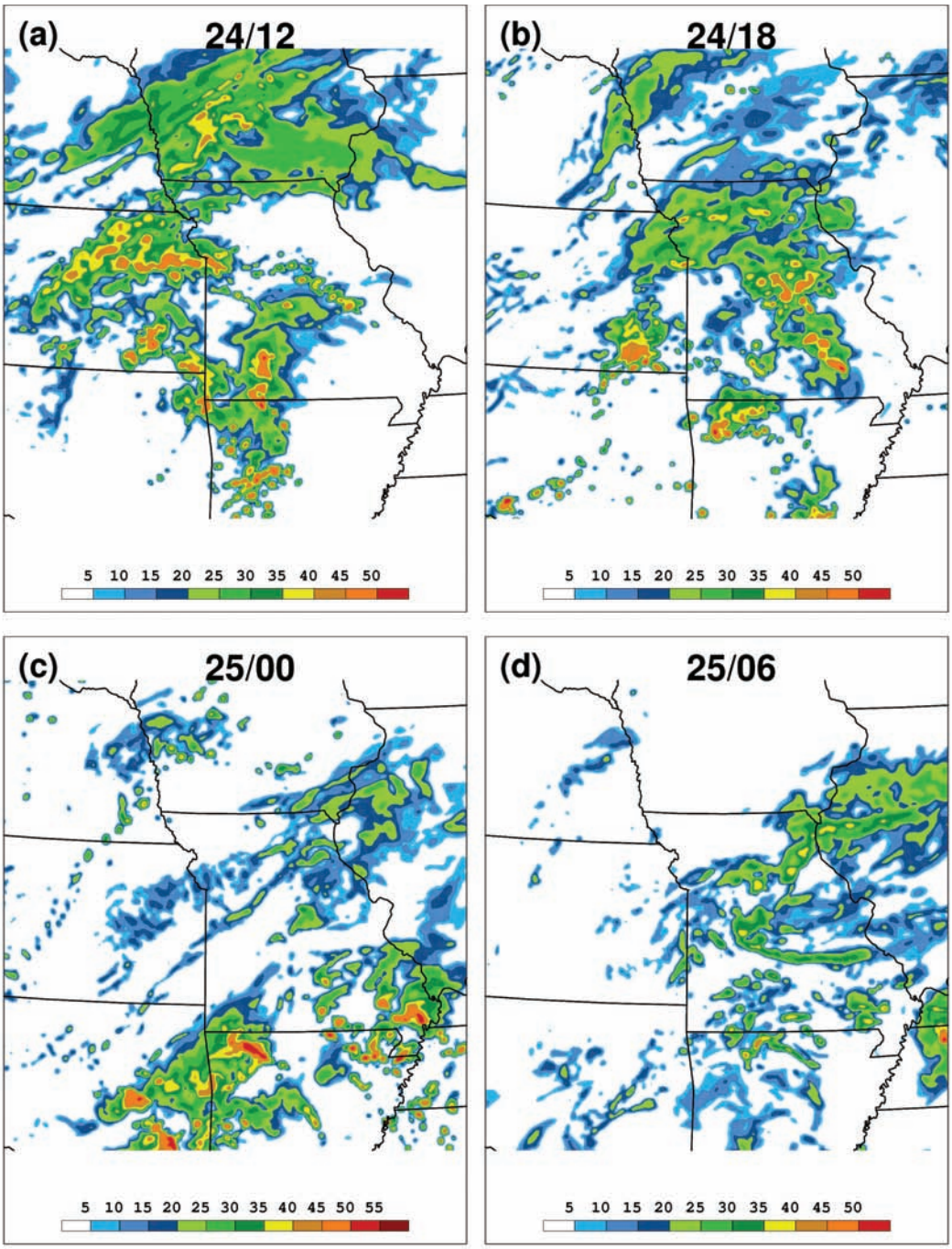

Fig. 14. As in Fig. 10, but using only ARW-4-WSM.

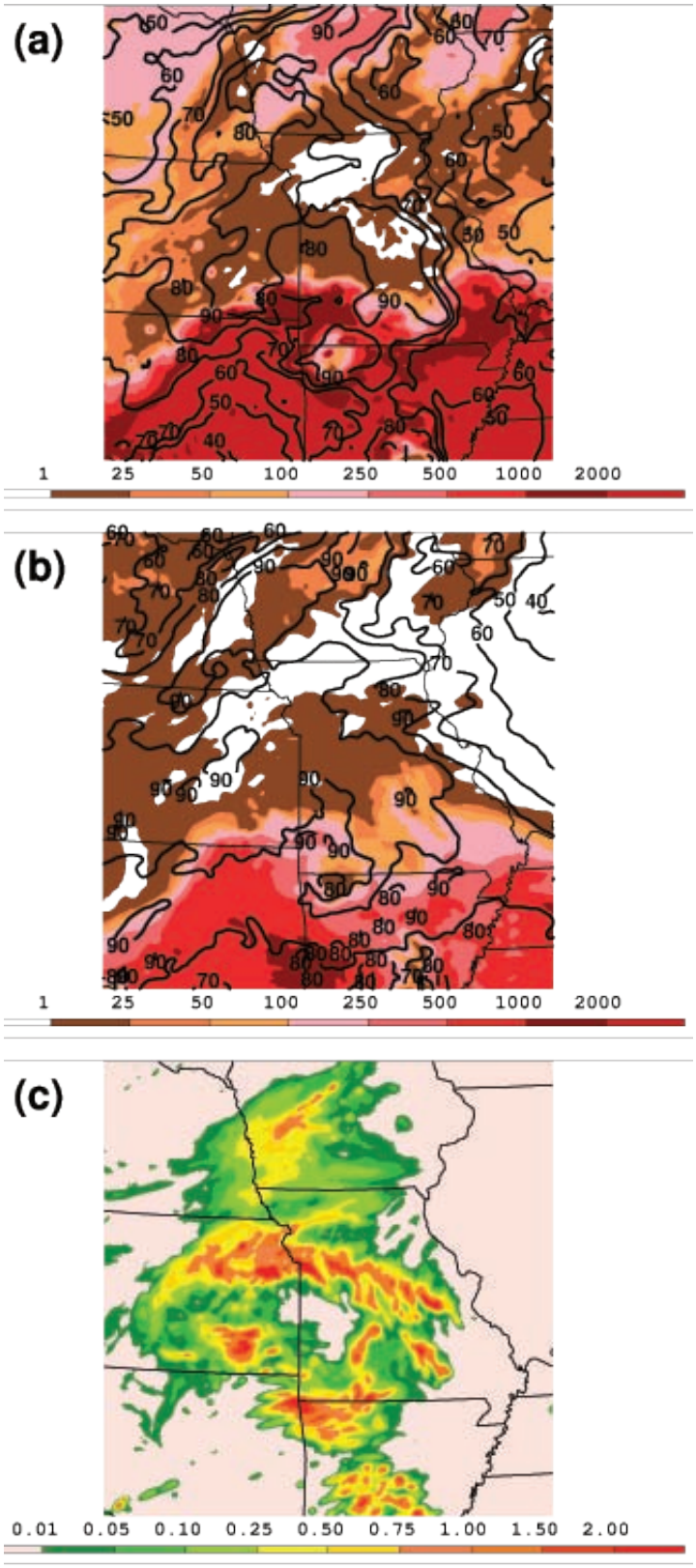

Fig. 15. As in Fig. 6, but using only ARW-4-WSM.

c. 2 km run

The simulation at 2 km provides nearly identical forecast guidance in terms of QPF (Fig. 17) as the ARW-4-WSM forecast (Fig. 13b), although some differences are noted in Oklahoma and Arkansas along the southern track of precipitation. This is as expected, as similar results were reported for a larger number of cases by Kain et al. (2008) and Schwartz et al. (2009). While the structure of the precipitation field has more detail, which may mimic what occurs in nature, the accuracy of the forecast is largely unchanged. It is clear that the forecast of this event did not benefit from the nearly tenfold increase in computer resources needed to create it.

5. Discussion and Conclusions

The initial condition used by the 2004 Eta was poor, and the CP scheme failed to predict the eastward propagation

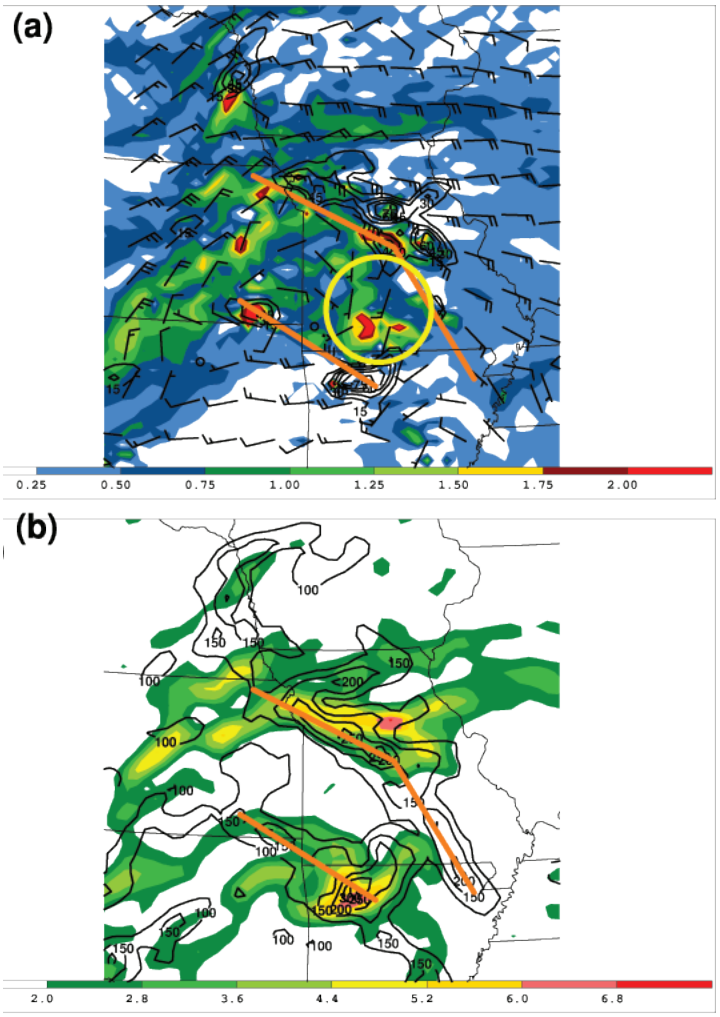

Fig. 16. As in Fig. 7, but using only ARW-4-WSM. Contour intervals for frontogenesis and deformation are the same as those in Fig. 12.

of convection. Though the precipitation forecast from the ARW-BMJ may not have been any more accurate than that of the 2004 Eta, it did feature a more realistic depiction of two separate tracks or instances of precipitation. This information would no doubt benefit operational forecasters, and is a testament to improvements in modeling over the past six years. The ARW-4-WSM considerably improved the precipitation forecast, as the convection-allowing grid spacing of the model eliminated the problems associated with the parameterization of convection, particularly those related to propagation. This improvement occurred despite the same rather poor initial condition being used. A better analysis would likely improve the forecast further. The ARW-2-WSM forecast did not provide enhanced forecast guidance in light of the large increase in computational resources needed to create it, a result similar to that found in previous studies. An interesting result from the ARW-4-WSM was the correlation between the intensification of convection and the development of frontogenesis. It was speculated that the convection itself contributed to this frontogenesis, via deformation induced by diabatically-generated PV anomalies. This was observed in the RUC analyses as well. In contrast with all other forecasts, the LLJ in the ARW-4-WSM became perpendicular to the frontogenesis and associated convection, rather than parallel. The reason for this is not clear, but may be associated with convection occurring at the same time farther south in a higher CAPE environment.

Although idealized simulations show that elevated convection can exist and propagate without the presence of a thermal boundary aloft (Parker 2008), real-data composites indicate that such a boundary is often present (Moore et al. 2003). Coniglio et al. (2010a) show that frontogenesis aloft commonly develops prior to and ahead of strong, long-lasting, nocturnal MCSs. In the July 2004 MCS analyzed here, frontogenesis aloft occurred only when convection approached the thermal gradient in central Missouri. This MCS was long-lasting, but was weaker and during the daytime. The relationship between frontogenesis and convection seen here may be an artifact of the atypical environment observed in this case. Nevertheless, the influence of convection on frontogenesis requires further investigation. Baxter et al. (2011) shows that in the model atmosphere, diabatic heating can contribute to frontogenesis that then focus and reinforces precipitation. If the model does not capture the propagation of convection well, this could lead to the improper development of frontogenesis which will then reinforce the errant propagation. Wang and Clark (2010) show that the operational NAM exhibits an over-prediction of deformation and convergence, leading to an over-prediction of precipitation. The reasons for this

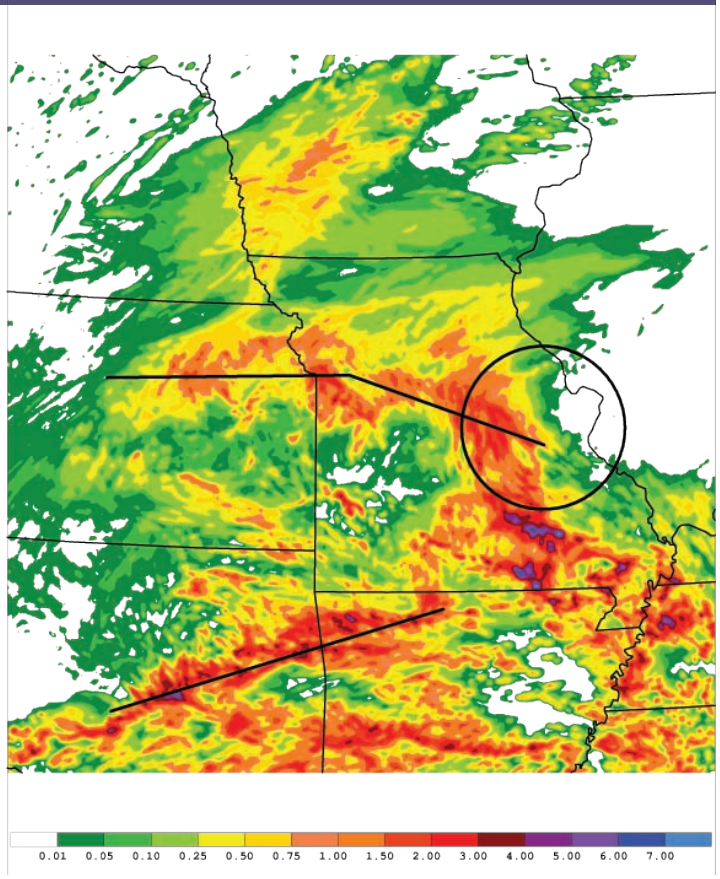

Fig. 17. As in Fig. 2, but using only ARW-2-WSM.

phenomenon are unknown, but may relate to the use of CP. Results from the July 2004 case presented here suggest that when such a situation arises in the model it will be self-reinforcing.

This study analyzes a single event that, while not extreme in terms of the amount of rainfall, may be particularly difficult for models containing CP to predict. Two separate convective events occurring in close proximity in space and time, and the weak forcing and instability present combine to give a variety of model solutions. The higher resolution forecast in this case gave solutions that were considerably different than the more coarse resolution models. Previous research suggests that this result is outside of the norm. Weisman et al. (2008) and Coniglio et al. (2010b) demonstrate that errors in the larger scales of forcing contained in the initial conditions from the operational NAM exert an overriding influence on the accuracy of the higher resolution model. However, the case presented here features weak forcing and small amounts of instability, possible reasons that allowed improved resolution and lack of a CP scheme to provide more substantial benefit.

The availability of models with and without CP may present challenges in the operational environment, as a convection-allowing model will not offer improved guidance for every event. As such, further case-study

comparisons of convection-allowing models with models using CP are warranted, in addition to forecaster training on how best to incorporate the results of these models in the decision making process.

Author

Marty Baxter is an Assistant Professor of Meteorology at Central Michigan University, where he is the primary instructor for Synoptic Meteorology. He received a BS from the University of Missouri in 2001, and an MS and PhD from Saint Louis University in 2003 and 2006, respectively. His current research interests include precipitation systems and the use of numerical weather prediction in operational forecasting. Dr. Baxter currently serves as the Editor of the NWA's Electronic Journal of Operational Meteorology, and as a member of the NWA's Weather Analysis and Forecasting Committee.

Acknowledgments

The author thanks Michelle Keast-Nachtrab for her efforts in support of this study in its earliest stages. RUC data were acquired from the Department of Energy's Atmospheric Radiation Program. Precipitation data were acquired from NCAR/EOL under sponsorship of the National Science Foundation. Thank you to Patrick Market for conducting a fruitful pre-review of the paper. The helpful comments from Joshua Scheck and Wayne MacKenzie during the review process improved the manuscript.

References

Anderson, C. J., W. A. Gallus Jr., R. W. Arritt, and J. S. Kain, 2002: Impact of adjustments in the Kain-Fritsch convective scheme on QPF of elevated convection. Preprints, *19th Conf. on Weather Analysis and Forecasting/15th Conf. on Numerical Weather Prediction*. Amer. Meteor. Soc., San Antonio, TX, Amer. Meteor. Soc., 23-24.

Baxter, M. A., P. N. Schumacher, and J. M. Boustead, 2011: The use of potential vorticity inversion to evaluate the effect of precipitation on downstream mesoscale processes. *Quart. J. Roy. Meteor. Soc.*, 137, 179-198.

Belair, S., and J. Mailhot, 2001: Impact of horizontal resolution on the numerical simulation of a midlatitude squall line: Implicit versus explicit condensation. *Mon. Wea. Rev.*, 129, 2362-2376.

Benjamin, S. G., G. G. Grell, J. M. Brown, T. G. Smirnova, and R. Bleck, 2004: Mesoscale weather prediction with the RUC hybrid isentropic-terrain-following coordinate model. *Mon. Wea. Rev.*, 132, 473-494.

Black, T. L., 1994: The new NMC Eta model: Description and forecast examples. *Wea. Forecasting*, 9, 265-278.

Brennan, M. J. and G. M. Lackmann, 2005: The influence of incipient latent heat release on the precipitation distribution of the 24-25 January 2000 U.S. east coast cyclone. *Mon. Wea. Rev.*, 133, 1913-1937.

Bryan, G. H., J. C. Wyngaard, and J. M. Fritsch, 2003: Resolution requirements for the simulation of deep moist convection. *Mon. Wea. Rev.*, 131, 2394-2416.

Carbone, R. E., J. D. Tuttle, D. A. Ahijevych, and S. B. Trier, 2002: Inferences of predictability associated with warm season precipitation episodes. *J. Atmos. Sci.*, 59, 2033-2056.

Carlson, T. N., 1991: *Mid-Latitude Weather Systems*. HarperCollins Academic, 507 pp.

Clark, A. J., W. A. Gallus Jr., and T.-C. Chen, 2007: Comparison of the diurnal precipitation cycle in convection-resolving and non-convection-resolving mesoscale models. *Mon. Wea. Rev.*, 135, 3456-3473.

Colman, B. R., 1990a: Thunderstorms above frontal surfaces in environments without positive CAPE. Part I: A climatology. *Mon. Wea. Rev.*, 118, 1103-1122.

_____, 1990b: Thunderstorms above frontal surfaces in environments without positive CAPE. Part II: Organization and instability mechanisms. *Mon. Wea. Rev.*, 118, 1123-1144.

Coniglio, M. C., J. Y. Hwang, and D. J. Stensrud, 2010a: Environmental factors in the upscale growth and longevity of MCSs derived from Rapid Update Cycle analyses. *Mon. Wea. Rev.*, 138, 3514-3539.

_____, K. L. Elmore, J. S. Kain, S. J. Weiss, M. Xue, and M. L. Weisman, 2010b: Evaluation of WRF model output for severe-weather forecasting from the 2008 NOAA Hazardous Weather Testbed Spring Experiment. *Wea. Forecasting*, 25, 408-427.

Corfidi, S. F., S. J. Corfidi, and D. M. Schultz, 2008: Elevated convection and castellanus: Ambiguities, significance, and questions. *Wea. Forecasting*, 23, 1280-1303.

Davis, C. A., and K. A. Emanuel, 1991: Potential vorticity diagnostics of cyclogenesis. *Mon. Wea. Rev.*, 119, 1929-1953.

_____, K. W. Manning, R. E. Carbone, S. B. Trier, and J. D. Tuttle, 2003: Coherence of warm season continental rainfall in numerical weather prediction models. *Mon. Wea. Rev.*, 131, 2667-2679.

Done, J., C. Davis, and M. Weisman, 2004: The next generation of NWP: Explicit forecasts of convection using the Weather Research and Forecasting (WRF) model. *Atmos. Sci. Lett.*, 5 (6), 110-117.

Doswell, C. A., III, H. E. Brooks, and R. A. Maddox, 1996: Flash flood forecasting: An Ingredients-based methodology. *Wea. Forecasting*, 11, 560-581.

Ek, M. B., K. E., Mitchell, Y. Lin, E. Rogers, P. Grunmann, V. Koren, G. Gayno, and J. D. Tarpley, 2003: Implementation of Noah land surface model advances in the National Center for Environmental Prediction operational mesoscale Eta model. *J. Geophys. Res.*, 108, 8851.

Ferrier, B. S., Y. Jin, Y. Lin, T. Black, E. Rogers, and G. DiMego, 2002: Implementation of a new grid-scale cloud and precipitation scheme in the NCEP Eta model. Preprints, *19th Conf. on Weather Analysis and Forecasting/15th Conf. on Numerical Weather Prediction*, Amer. Meteor. Soc., San Antonio, TX, Amer. Meteor. Soc., 280-283.

Fritsch, J. M., and R. E. Carbone, 2004: Improving quantitative precipitation forecasts in the warm season. *Bull. Amer. Meteor. Soc.*, 85, 955-965.

Gallus, W. A., Jr., 1999: Eta simulations of three extreme rainfall events: Impact of resolution and choice of convective scheme. *Wea. Forecasting*, 14, 405-426.

_____, and M. Segal, 2001: Impact of improved initialization of mesoscale features on convective system rainfall in 10-km Eta simulations. *Wea. Forecasting*, 17, 192-205.

Glickman, T. S., Ed., 2000: *Glossary of Meteorology*. 2nd Ed. Amer. Meteor. Soc., 855 pp.

Hong, S.-Y., J. Dudhia, and S.-H. Chen, 2004: A revised approach to ice-microphysical processes for the bulk parameterization of clouds and precipitation. *Mon. Wea. Rev.*, 132, 103-120.

Hoskins, B. J., M. E. McIntyre, and A. W. Robertson, 1985: On the use and significance of isentropic potential vorticity maps. *Quart. J. Roy. Meteor. Soc.*, 111, 877-946.

Janjic, Z. I., 1994: The step-mountain Eta coordinate model: Further developments of the convection, viscous sublayer, and turbulence closure schemes. *Mon. Wea. Rev.*, 122, 927-945.

Jankov, I,, and W. A. Gallus Jr., 2004: MCS rainfall forecast accuracy as a function of large-scale forcing. *Wea. Forecasting*., 19, 428-439.

Kain, J. S., 2004: The Kain-Fritsch convective parameterization: An update. *J. Appl. Meteor.*, 43, 170-181.

_____, S. J. Weiss, J. J. Levit, M. E. Baldwin, and D. R. Bright, 2006: Examination of convection-allowing configurations of the WRF model for the prediction of severe convective weather: The SPC/NSSL Spring Program 2004. *Wea. Forecasting*, 21, 167-181.

_____, and Coauthors, 2008: Some practical considerations regarding horizontal resolution in the first generation of operational convection-allowing NWP. *Wea. Forecasting*, 23, 931-952.

Kleinschmidt, E., 1957: Cyclones and anticyclones. *Dynamic Meteorology, Handbuch der Physik,* S. Flugge, Ed., Springer-Verlag, 48, 112-154.

Koch, S. E., B. Ferrier, M. Stoelinga, E. Szoke, S. J. Weiss, and J. S. Kain, 2005: The use of simulated radar reflectivity fields in the diagnosis of mesoscale phenomena from high-resolution WRF model forecasts. Preprints, *12th Conf. on Mesoscale Processes*, Albuquerque, NM, Amer. Meteor. Soc., J4J.7.

Korner, S. O., and J. E. Martin, 2000: Piecewise frontogenesis from a potential vorticity perspective: Methodology and a case study. *Mon. Wea. Rev.*, 128, 1266-1288.

Lacis, A. A. and J. Hansen, 1974: A parameterization for the absorption of solar radiation in the Earth's atmosphere. *J. Atmos. Sci.*, 31, 118-133.

Lackmann, G. M., 2002: Cold-frontal potential vorticity maxima, the low-level jet, and moisture transport in extratropical cyclones. *Mon. Wea. Rev.*, 130, 59-74.

Lin, Y. and K. E. Mitchell, 2005: The NCEP Stage II/IV hourly precipitation analyses: Development and applications. Preprints, *19th Conf. on Hydrology*, San Diego, CA, Amer. Met. Soc., 1.2.

Liu, C., M. W. Moncreiff, J. D. Tuttle, and R. E. Carbone, 2006: Explicit and parameterized episodes of warm-season precipitation over the continental United States. *Adv. Atmos. Sci.*, 23, 91-105.

Mellor, G. L., and T. Yamada, 1982: Development of a turbulence closure model for geophysical fluid problems. *Rev. Geophys. Space Phys.*, 20, 851-875.

Moore, J. T., F. H. Glass, C. E. Graves, S. M. Rochette, and M. J. Singer, 2003: The environment of warm-season elevated thunderstorms associated with heavy rainfall over the central United States. *Wea. Forecasting*, 18, 861-878.

Morgan, M. C., 1999: Using piecewise potential vorticity inversion to diagnose frontogenesis, Part I: A partitioning of the Q vector applied to diagnosing surface frontogenesis and vertical motion. *Mon. Wea. Rev.*, 127, 2796-2821.

Novak, D. R., B. A. Colle, and R. McTaggart-Cowan, 2009: The role of moist processes in the formation and evolution of mesoscale snowbands within the comma-head of Northeastern United States cyclones. *Mon. Wea. Rev.* 137, 2662-2686.

Olson, D. A., N. W. Junker, and B. Korty, 1995: Evaluation of 33 years of quantitative precipitation forecasting at the NMC. *Wea. Forecasting,* 10, 498-511.

Orville, R. E., and G. R. Huffines, 2001: Cloud-to-ground lightning in the United States: NLDN results in the first decade, 1989-98. *Mon. Wea. Rev.*, 129, 1179-1193.

Parker, M. D., 2008: Response of simulated squall lines to low-level cooling. *J. Atmos. Sci.*, 65, 1323-1341.

Petch, J. C., 2006: Sensitivity studies of developing convection in a cloud-resolving model. *Quart. J. Roy. Meteor. Soc.*, 132, 345-358.

Raymond, D. J., and H. Jiang, 1990: A theory for long-lived mesoscale convective systems. *J. Atmos. Sci.*, 47, 3067-3077.

Rochette, S. M., and J. T. Moore, 1996 : Initiation of an elevated mesoscale convective system associated with heavy rainfall. *Wea. Forecasting*, 18, 861-878.

Schwartz, C. S., J. S. Kain, S. J. Weiss, M. Xue, D. R. Bright, F. Kong, K. W. Thomas, J. J. Levit and M. C. Coniglio, 2009: Next-day convection-allowing WRF model guidance: A second look at 2 vs 4 km grid spacing. *Mon. Wea. Rev.*, 137, 3351-3372.

Skamarock, W. C., 2004 : Evaluating mesoscale NWP models using kinetic energy spectra. *Mon. Wea. Rev.*, 132, 3019-3032.

_____, and coauthors, 2008 : A description of the advanced research WRF Version 3, 113 pp. [Available online at: http://www.mmm.ucar.edu/wrf/users/docs/arw_v3.pdf]

Thompson, R. L., C. M. Mead, and R. Edwards, 2007: Effective storm-relative helicity and bulk shear in supercell thunderstorm environments. *Wea. Forecasting*, 22, 102-115.

Trier, S. B., and D. B. Parsons, 1993: Evolution of environmental conditions preceding the development of a nocturnal mesoscale convective complex. *Mon. Wea. Rev.*, 121, 1078-1098.

_____, C. A. Davis, D. A. Ahijevych, M. L. Weisman, and G. H. Bryan, 2006: Mechanisms supporting long-lived episodes of propagating nocturnal convection within a 7-day WRF model simulation. *J. Atmos. Sci.*, 63, 2437-2461.

Tuttle, J. D., and C. A. Davis, 2006: Corridors of warm season precipitation in the central United States. *Mon. Wea. Rev.*, 134, 2297-2317.

Vasic, S., C. A. Lin, I. Zawadkzi, O. Bosquet, and D. Chaumont, 2007: Evaluation of precipitation from numerical weather prediction models and satellites using values retrieved from radars. *Mon. Wea. Rev.*, 135, 3750-3766.

Wang, W., and N. L. Seaman, 1997: A comparison study of convective schemes in a mesoscale model. *Mon. Wea. Rev.*, 125, 252-278.

Wang, S.-Y., and A. J. Clark, 2010: NAM model forecasts of warm season quasi-stationary frontal environments in the central United States. *Wea. Forecasting*, 25, 1281-1292.

Weisman, M. L., W. C. Skamarock, and J. B. Klemp, 1997: The resolution dependence of explicitly simulated squall lines. *Mon. Wea. Rev*., 125, 527-548.

_____, C. Davis, W. Wang, K. W. Manning, and J. B. Klemp, 2008: Experiences with 0-36 h explicit convective forecasts with the WRF-ARW model. *Wea. Forecasting*, 23, 407-437.

Wilson, J. W., and R. D. Roberts, 2006: Summary of convective storm initiation and evolution during IHOP: Observational and modeling perspective. *Mon. Wea. Rev.*, 134, 23-47.

Zhang, D.-L., E.-Y. Hsie, and M. W. Moncreiff, 1988: A comparison of explicit and implicit predictions of convective and stratiform precipitating weather systems with a meso-β-scale numerical model. *Quart. J. Roy. Meteor. Soc.*, 114, 31-60.